THE EFFECT OF UNIFORMLY DISTRIBUTED ROUGHNESS ON TURBULENT SKIN FRICTION DRAG AT SUPERSONIC SPEEDS

Thesis by

Frank E. Goddard, Jr.

In Partial Fulfillment of the Requirements

For the Degree of

Doctor of Philosophy

California Institute of Technology

Pasadena, California

1957

ACKNOWLEDGMENTS

The author wishes to express his appreciation to Professor H. W. Liepmann for his help and guidance throughout this investigation. He is grateful also for discussions with Professor Lester Lees and Drs. J. Laufer and P. Wegener.

Very much assistance was rendered by the staff of the Wind Tunnel Section at the Jet Propulsion Laboratory on many occasions.

The author also thanks Marcella H. Callahan for her help and diligence in typing and preparing the manuscript.

ABSTRACT

An experimental program was carried out in the 18 x 20-inch supersonic wind tunnel of the Jet Propulsion Laboratory at the California Institute of Technology to determine the effect of uniformly distributed sand-grain roughness on the skin friction drag of a body of revolution for the case of a turbulent boundary layer. The Mach-number range covered was 1.98 to 4.54 and the Reynolds number varied from about 3×10^6 to 8×10^6. Some data were also obtained at a Mach number of 0.70.

At speeds up to a Mach number of 5 and for roughness sizes such that the quadratic resistance law holds, the compressibility effect is indirect and the skin friction drag is a function only of the roughness Reynolds number, $\frac{v_* k}{\nu}$, just as in the incompressible case.

The critical roughness below which the surface is hydraulically smooth is $k_{critical} \cong \frac{10\,\nu}{v_*}$ and this is equal to the thickness of the laminar sublayer for a smooth surface for both compressible and incompressible flows.

Over the range of roughness sizes considered here there appears to be no wave drag associated with the drag due to roughness.

The shift in the turbulent velocity profile $\Delta \frac{u}{v_*}$ for a rough surface at supersonic speeds is a function only of the roughness Reynolds number, $\frac{v_* k}{\nu}$, and quantitatively follows identically the same law as in the incompressible case.

TABLE OF CONTENTS

LIST OF FIGURES

LIST OF FIGURES (Cont'd)

LIST OF FIGURES (Cont'd)

I. INTRODUCTION

The effect of surface roughness on the skin friction drag of the surface is of great practical importance in the fields of aeronautical, marine and hydraulic engineering, since in the first two cases it is related to the performance possibilities of aircraft and ships, and in the third case it is related to the efficiency of hydraulic machinery and installations. It is also of fundamental interest as a problem in fluid mechanics.

Various aspects of the problem have been treated by many investigators in the low-speed, incompressible case. The most systematic experimental investigation of both the skin friction drag and the development of the boundary-layer structure on a rough surface was carried out by J. Nikuradse (ref. 1). His tests were made with water flowing at low speeds through cylindrical pipes, whose interior walls were artificially roughened using closely packed sand grains. More recently, experiments have been carried out at the Iowa Institute of Hydraulic Research and reported in a very interesting paper by F. R. Hama (ref. 2). The main results are concerned with the effect of roughnesses of different kinds on the boundary-layer velocity profile. General skin friction drag formulae are deduced from the velocity profile laws but no direct skin friction drag measurements were made. A summary of the present state of knowledge of the turbulent boundary layer for the low-speed case, including the effects of roughness, is to be found in the excellent paper by F. H. Clauser (ref. 3).

It is interesting to observe that during the past thirty years research work on roughness effects has been piecemeal and the only really systematic investigation, that of Nikuradse (ref. 1), was done with pipe flow. The resistance charts prepared by Prandtl and Schlichting (ref. 4) were developed from Nikuradse's pipe data and involve the tacit assumption that the roughness effect would be universal and independent of outside flow conditions. To this day there do not exist, to the writer's knowledge, any direct skin friction drag measurements for a low-speed boundary-layer flow with a rough surface. The writer has learned recently that a systematic program of direct drag measurements on the flat wall of a low-speed wind tunnel with rough surfaces is now under way at the Aerodynamics Institute in Göttingen (1957).

The one piece of work done at supersonic speeds on the drag of rough surfaces, to the writer's knowledge, is that of Wade at the University of Toronto (ref. 5). Here the critical roughness size which causes a drag increase above that of a smooth surface was found for a screw-thread roughness at a single Mach number of 2.48 and one Reynolds number.

It was the purpose of the present investigation to determine experimentally the manner in which the turbulent skin friction drag of rough surfaces varies with Mach number and Reynolds number in the supersonic speed range and to compare these results with the available incompressible results. Such a comparison will show whether any new phenomena are involved in the compressible case. It was intended to find also the critical permissible roughness of a surface up to which the skin friction drag is the same as a smooth surface. Finally, it was planned to make boundary-layer-profile measurements to ascertain in what manner the boundary-layer structure is different from the incompressible case.

II. EXPERIMENTAL PROGRAM

A. Skin Friction Drag Measurements

1. The JPL 18 x 20-inch supersonic wind tunnel. The tests to be described were carried out in the 18 x 20-inch supersonic wind tunnel at the California Institute of Technology's Jet Propulsion Laboratory. It is a continuous-flow tunnel with an 18 x 20-inch test section and operates from a Mach number of about 1.3 to 5.0. The supply pressure may be varied so that the Reynolds number can be varied from about 120,000 to about 400,000 per inch of characteristic length. The nozzle of the tunnel is a pair of flexible steel plates set to shape by twenty-two pairs of motor-operated jacks, and thus the tunnel may be run at any Mach number in the range 1.3 to 5.0. The Mach number is uniform in the test section to within ±.01 and the static pressure is uniform to within about ±1 per cent. The flow is parallel throughout the test section to within about ±0.1 degrees. At the present state of the art of wind-tunnel design, it can be said that this tunnel has a very high degree of flow uniformity. A photograph of the nozzle looking upstream from the test section is shown in figure 1. One of the side plates has been removed.

2. Technique. The technique used for the drag measurements was selected because of its directness, simplicity and adaptability to the wind tunnel and balance systems available. The models were bodies of revolution consisting of a smooth ogival nose piece followed by a cylindrical afterbody. The cylindrical afterbody was carefully wrapped with high-grade commercial sandpaper with sand grains of several different average sizes. A front-lighted schlieren photograph of a typical model installed in the test section of the tunnel with the wind on is shown in

figure 2. The drag measuring technique is exactly that used by Chapman and Kester (ref. 6). It consists in testing the complete model during which the total drag and base pressure are both measured (figs. 3 and 3a). From these two drag measurements the fore drag of the complete model is found.

$$D_{T_1} - D_{B_1} = D_{F_1} \tag{1}$$

Next, the smooth ogival nose is tested alone, the total drag and base pressure being again measured (figs. 4 and 4a). From these two drag measurements the fore drag of the ogival nose is then found.

$$D_{T_2} - D_{B_2} = D_{F_2} \tag{2}$$

Finally, by subtracting the fore drag of the ogival nose from the fore drag of the complete model, the resulting skin friction drag of the cylindrical afterbody is found.

$$D_{F_1} - D_{F_2} = D_{SF} \tag{3}$$

The average skin friction drag coefficient of the cylindrical afterbody is determined based on the wetted area of the cylindrical afterbody, and the Reynolds number corresponding thereto is determined based on the free-stream velocity V and the longitudinal length ℓ of the cylindrical afterbody. d is the body diameter.

$$C_F = \frac{(D_{SF} + \Delta D)}{\frac{\rho}{2} V^2 \pi d \; (\ell + \Delta \ell)} \; ; \qquad R = \frac{V \; (\ell + \Delta \ell)}{\nu} \tag{4}$$

Now in all cases the boundary layer of the ogival nose was made fully turbulent by means of a small wire ring placed at the nose of the ogive.

In this fashion it was certain that the boundary layer over the rough cylinder was fully turbulent at all times. Both the trip wire near the nose and the resulting turbulent state of the boundary layer can be seen in figures 2, 3, and 4.

Because the turbulent boundary layer was thus of finite thickness at the front end of the rough-surfaced afterbody, it was necessary to find the effective length of the cylinder by adding a length $\Delta\ell$ to the geometric length ℓ equal to the calculated fictitious "starting length" of the cylinder which would produce the actually observed boundary-layer thickness that existed at the front end of the cylindrical afterbody. ΔD is the drag corresponding to $\Delta\ell$. In this way, both the average drag coefficient and the Reynolds number were corrected to "effective" values as shown in equation 4. The calculation of $\Delta\ell$ and ΔD is shown on page 9.

A total of eight rough-surfaced cylindrical afterbodies and one smooth one were used together with a single smooth ogival nose piece to form nine models. The root-mean-square average sand-grain diameter k, in inches, for the models used was as follows:

k = 0 (smooth)
= 0.0008 inches
= 0.0027 inches
= 0.0039 inches
= 0.0066 inches
= 0.0095 inches
= 0.0131 inches
= 0.0240 inches
= 0.0380 inches

Each cylindrical afterbody was undercut by an amount equal to the combined thickness of the sand plus glue plus paper which makes up the sandpaper. Thus the tops of the sand grains on the cylinder are a flush continuation of the smooth surface of the ogival nose at its base.

Two balance systems were used during the investigation. The first one is the regular external, six-component, mechanical-hydraulic balance with which the wind tunnel is regularly equipped. It is built in to the tunnel proper and is shown schematically in figure 5. A photograph of the balance outside the tunnel is shown in figure 6. The model is always at zero angle of attack and yaw and so, for purposes of this investigation, only the drag component was used. The model drag pushes the entire balance and suspension system downstream, and this motion is resisted by the hydraulic load cell marked "D" in figure 5. The model plus sting, sector, sector bearings, moment table, pyramidal struts, force table and drag link are all solidly connected and move downstream as a unit. The drag link connecting the force table to the drag cell "D" can be seen in figure 5. The balance is very reliable and repeatable and its accuracy is discussed on page 16.

It will be recognized that, since the skin friction drag is found from a double subtraction of four measured quantities, and since there is a large change in dynamic pressure as one changes the Mach number from 2 to 5 and the Reynolds number by a factor of four, at the start of the investigation there was some concern about the accuracy of a fixed range balance, which the JPL balance is. And so a second balance was used, at the beginning of the program, which had been especially designed as a single-component, variable range spring balance. This balance was designed and built by Mr. J. M. Kendall of the U. S. Naval Ordnance Laboratory in

White Oak, Maryland. It had been known to the writer because of its previous and successful use at NOL. The writer would like to express here his great appreciation to Dr. H. Kurzweg and Mr. Kendall of NOL for the loan of the NOL balance over an extended period of time and to thank Mr. Kendall for his help during a week which he spent at JPL and instructed JPL personnel in its use. A sketch of the balance is shown in figures 7 and 7a. The balance is fully described in reference 13. It will be seen that it is simply a direct spring balance. The sliding friction is minimized by rotating the bearings which support the model sting with an electric motor. The balance load range is changed by inserting a spring of the appropriate stiffness. The sting deflection axially is measured by the stem attached to the sting frame. The stem is inside the field of a Schaevitz coil which electrically picks up its motion. Outside the tunnel a reader box contains a second Schaevitz coil and a finely divided micrometer which through a lever and gears moves a stem in the coil. With no drag applied, the two coils are electrically nulled with the spring unloaded. When the tunnel is turned on and the drag applied, the force extends the spring and upsets the balance between the two coils. One then rotates the micrometer manually until the output of the two coils are again nulled and the micrometer drum rotation to balance is proportional to the drag. The whole system is mechanically and electrically calibrated.

The model with sting and balance box is shown in figure 8 and its installation in the tunnel in figure 9. In figure 10 is shown a close-up of the sting-model connection and the annular gap through which the base pressure is led inside the model, from which it goes out through the sting to the balance box and to the tunnel sector-windshield, whence it goes out of the tunnel to a manometer for recording.

Figure 11 shows a schematic diagram of the reader. Figure 12 shows the reader box containing micrometer and second coil and the associated electrical equipment needed for power supply, voltage and voltage balance indication between the two coils.

3. Data reduction and corrections. The essential steps in the data reduction process have already been indicated in the previous section in equations 1 to 4. A typical set of raw data as directly obtained during the wind-tunnel test procedure is shown in figures 13 to 16. In these plots the base drag has already been subtracted from the measured total drag to give the fore drag. p_t is the tunnel supply pressure in centimeters of mercury. The uncorrected skin friction coefficient is obtained immediately after equation 3.

$$C_F = \frac{\dfrac{D_{SF}}{p_t}}{\dfrac{q}{p_t}} \quad \frac{1}{\pi d \ell}$$

For all models $\ell = 14$ inches and $d = 2$ inches. q/p_t is obtained from standard compressible flow tables for the Mach number concerned. $q = \frac{\rho}{2} V^2$. V is computed from the Mach number and tunnel supply temperature.

The effective "starting length" correction, $\Delta \ell$, due to the finite boundary-layer thickness at the front end of the cylindrical afterbody, and the skin friction drag correction, ΔD, corresponding to $\Delta \ell$ are found as follows:

By equating the sum of the local skin friction drag up to a station x on a surface to the loss of momentum in the boundary layer at x we obtain

$$D(x) = \pi d \int_0^x \tau_0 (x)\, dx = \pi d \rho \int_0^{\delta(x)} u (V - u)\, dy$$

but θ, the boundary-layer momentum thickness is

$$\theta = \frac{1}{V^2} \int_0^{\delta(x)} u (V - u)\, dy$$

and so

$$D(x) = \pi d \rho V^2 \theta$$

Now $C_F = \dfrac{D(x)}{\frac{\rho}{2} V^2 \pi d x} = \dfrac{\pi d \rho V^2 \theta}{\frac{\rho}{2} V^2 \pi d x} = \dfrac{2\theta}{x}$

therefore

$$\Delta \ell = \frac{2\theta}{C_F} \qquad (5)$$

and $\Delta D = \pi d \rho V^2 \theta$ (6)

These are the corrections in equation 4.

In the present investigation the boundary-layer thickness δ at the front end of the cylindrical afterbody was measured optically and θ found from

$$\theta = \frac{\delta_{\text{measured}}}{(\delta/\theta)}$$

The denominator is the calculated ratio of δ/θ for a 1/7th power law turbulent boundary layer at supersonic speeds (ref. 7).

In equation 5, C_F is the average turbulent skin friction drag coefficient for a rough surface at a Reynolds number based on the length $\Delta \ell$ and the velocity at the edge of the boundary layer.

For the models used the length ℓ was 14 inches. The correction $\Delta \ell$ in equation 4 varied from 3 to 9 inches, depending on the Mach number, and ΔD was from 20 per cent to 50 per cent of D_{SF} depending on the Mach number.

The present tests were made using ogive-cylinder bodies of revolution. This was done because of the intrinsic ease and reliability of making the tests with such models, rather than with a two-dimensional model such as a flat plate. Now for long cylinders the boundary-layer thickness becomes comparable to the cylinder radius, and under these conditions appreciable departures from flat-plate skin friction values would be expected according to the analyses of Jakob and Dow (ref. 9) and Eckert (ref. 10). Chapman and Kester (ref. 6) showed experimentally that the skin friction drag coefficient for a cylinder with an ℓ/d of 23 was a little less than 5 per cent higher than for an ℓ/d of 8. Furthermore, Chapman and Kester obtained the same skin friction drag results with bodies of revolution as did Coles (ref. 8) using a flat plate. (See fig. 11 of ref. 6.) Finally, the ℓ/d for the models of the present investigation was 11.5 in all cases, and so it is concluded that the present models have a small enough ℓ/d so that the results are the same as those for a flat plate.

The calculation of the "roughness" Reynolds number, which will be shown to be important in the discussion of the results, is as follows:

$$\text{Roughness Reynolds number} = \frac{kv_*}{\nu}$$

where k = roughness height.

v_* = "friction" velocity = $\sqrt{\frac{\tau}{\rho}}$

ν = kinematic viscosity.

In calculating $\frac{kv_*}{\nu}$, wall values of all factors are used.

$$\frac{kv_*}{\nu} = \frac{k\sqrt{\frac{\tau_w}{\rho_w}}}{\nu_w} = \frac{k\sqrt{\frac{C_f \frac{\rho_o}{2} V_o^2}{\rho_w}}}{\nu_w} = \frac{k\,V_o\sqrt{\frac{C_f}{2}}\sqrt{\frac{\rho_o}{\rho_w}}}{\nu_w}$$

The subscript o means free-stream values.

Now assuming

a. Prandtl number = 1

b. $p = \rho RT$

c. p is constant across the boundary layer

d. $\mu \sim T^w$, where $w = .76$

and calling $\frac{1}{1 + \frac{\gamma - 1}{2} M^2} = A$

$$\therefore \quad \rho_w = A\rho_o$$

$$\nu_w = \frac{\nu_o}{A^{w+1}}$$

$$\frac{kv_*}{\nu} = \frac{k\ V_o \sqrt{\frac{C_f}{2}} \cdot \sqrt{\frac{1}{A}} \cdot A^{w+1}}{\nu_o} = \frac{k\ V_o \sqrt{\frac{C_f}{2}} \cdot A^{w+\frac{1}{2}}}{\nu_o}$$

$$\frac{kv_*}{\nu} = \frac{k\ V_o \sqrt{\frac{C_f}{2}}}{\nu_o \left(1+\frac{\gamma-1}{2} M^2\right)^{1.26}} \qquad (7)$$

C_f corresponds to a given k and M.

4. Skin friction drag results. The results of the drag measurements described above are plotted in figures 17 to 25. The data in figures 17 to 22 were obtained using the JPL balance, and the data in figures 23 to 25 were obtained using the NOL balance. In each of these figures, the average skin friction drag coefficient is plotted against the Reynolds number, based on the effective length of the cylindrical afterbody, for several values of the roughness size at a given Mach number. For purposes of comparison, there is included in each figure the skin friction drag of an aerodynamically smooth surface for the same Mach number, according to the measurements made by D. Coles in the same wind tunnel in 1952 and reported in reference 8. It is of immediate interest to compare the present measurements for a rough surface with the same measurements for a rough surface at Mach number M = 0. This is possible by using Nikuradse's data (ref. 1) which were discussed in the Introduction. These results were converted to the drag coefficient for a flat-plate boundary layer by Prandtl and Schlichting in reference 4. They are shown in figures 17 through 22 and are noted with the symbol P-S-N (M = 0). It can be seen immediately in figures 17 through 25 that at supersonic speeds the drag coefficient

decreases steadily as the Mach number is increased. A comparison between the present supersonic results and Nikuradse's results at Mach number M = 0 is made at the same values of ℓ/k, where ℓ is the effective longitudinal length of the cylindrical afterbody and k is the average sand-grain diameter.

In figure 26 there is shown the compressibility effect at supersonic speeds for rough surfaces. In this plot the results shown in figures 17 through 22 have been crossplotted at a Reynolds number of eight million. The ratio of the compressible skin friction coefficient determined in the present investigation to the incompressible skin friction coefficient as determined by Nikuradse is plotted against Mach number, and it is seen that the resulting curve is fair and that the variation with Mach number is similar to that determined experimentally by Coles (ref. 8) for the case of smooth surfaces. It is also apparent that the compressibility effect for rough surfaces is considerably greater than that for smooth surfaces. As a matter of interest, there is also included the estimate of the compressibility effect for smooth surfaces made by von Kármán in his 1935 Volta-Congress paper (ref. 11). It is important to point out that the skin friction drag ratio at each of the six Mach numbers of the present tests was independent of roughness size.

In figure 26a the compressibility effect is shown in a more directly physical way. If the roughness height is such that the skin friction drag is indeed quadratic then one may write

$$C_F = \frac{C_D \, n \, k \, \frac{1}{2} \rho_w \, u_k^2}{\frac{1}{2} \rho \, V^2}$$

where C_D = drag coefficient of a single sand grain.

n = number of sand grains per unit surface area.

k = roughness height.

ρ_w = density at the wall.

u_k = velocity at $y = k$.

ρ = density at the edge of the boundary layer.

V = velocity at the edge of the boundary layer.

and

$$C_{F_i} = \frac{C_D\, n\, k\, \frac{1}{2} \rho\, u_k^2}{\frac{1}{2} \rho\, V^2}$$

then

$$\frac{C_F}{C_{F_i}} = \frac{\rho_w}{\rho} = \frac{1}{1 + .86\, \frac{\gamma - 1}{2}\, M^2}$$

In this manner the data of figure 26 have been plotted in figure 26a and compared with the straight line relationship

$$\frac{C_F}{C_{F_i}} = \frac{\rho_{wall}}{\rho}$$

and indeed the comparison is excellent.

From this one can see that the skin friction drag of the rough surface is quadratic and that the compressibility effect is entirely a reduction of the density at the wall as the Mach number increases.

It would be interesting to see how the ratio of the compressible skin friction coefficient to the incompressible skin friction coefficient varies as the roughness size is steadily decreased from the "hydraulically" smooth condition to the aerodynamically smooth condition. This is shown in figure 27 using the data in figure 28. The data in figures 27 and 28 are taken from some measurements made by Wade at the Institute of Aerophysics at the University of Toronto at the single Mach number of 2.48 for very small roughnesses (ref. 5). It can be seen that the drag coefficient ratio increases from the roughness size which is "critical" down to the aerodynamically smooth case and that when $k = 0$ the drag coefficient ratio is the same as that determined by Coles for a smooth flat plate.

Figures 27 and 28 in fact lead to the following important observations:

1. It happens that Wade's "roughness" was a screw-thread roughness; that is, it was obtained by cutting a screw thread of peak-to-valley height k on the cylindrical portion of his model. Figure 28 shows that the drag increase due to a sand-grain roughness (JPL - fig. 19) is about the same as that due to a transverse screw-thread roughness of the same height k. The screw-thread roughness is two-dimensional.

2. Wade's model was a cone-cylinder model, and for the smooth case ($k = 0$) he obtained the same compressible-to-incompressible skin friction drag ratio as did Coles for a flat plate (fig. 27). Thus, we have an independent check on the previous demonstration that for suitable length-diameter ratios of bodies of revolution the skin friction drag is the same as on a flat plate.

3. Figure 28 shows that at $M \cong 2.5$ the critical roughness at which the surface becomes "hydraulically" smooth is about $k = 0.0008$ inches, and thus the values of C_F/C_{F_i} in figure 27 which are intermediate between the asymptotic value for large k and $k = 0$ correspond to "hydraulically" smooth surfaces. Finally, this means that the area between the "rough" and "smooth" compressibility effect curves in figure 26 corresponds to surfaces which have become "hydraulically" smooth in the compressible case (C_F) but are still "hydraulically" rough in the incompressible case (C_{F_i}) for the same value of ℓ/k.

In figure 29 the skin friction drag coefficients from the present tests have been plotted against Mach number at the Reynolds number of eight million and compared again with the values for a smooth surface as determined by Coles. It is clear that, as the Mach number increases, a surface of a given roughness becomes "hydraulically" smooth because of the growth of the boundary-layer thickness with increase in Mach number.

In figure 30 the skin friction drag coefficient is plotted against the roughness height at a Reynolds number of eight million for each of the six Mach numbers of the present tests.

In figure 31 there is shown a correlation of the results of figure 30 which is obtained by plotting the ratio of the skin friction drag coefficient for the rough surface to the value for the smooth surface versus the logarithm of the "roughness" Reynolds number kv_*/ν based on the roughness height k and the "friction velocity" v_*. The obviously successful correlation shown in figure 31, $C_F/C_{F_o} = f\left(\log \frac{kv_*}{\nu}\right)$, is the same functional relationship shown to hold in the incompressible case by Nikuradse (ref. 1) for closely packed sand-grain roughness.

5. Accuracy of the measurements. The accuracy problem and the accuracy actually achieved in these present tests will be demonstrated by considering two extreme cases from the present investigation; namely:

1. $M = 1.98$ and $k = .038$ inches

$p_t = 140$ cm Hg (supply pressure)

$D_{\text{Body \& Nose}} = .061 \times 140 = 8.53$ lbs

$D_{\text{Nose}} = .023 \times 140 = \underline{3.22}$ lbs

$\therefore D_{\text{Skin Friction}} = 5.31$ lbs

If $p_t = 45$ cm Hg, a minimum value at $M = 1.98$

$\therefore D_{\text{Skin Friction}} = 1.60$ lbs

2. $M = 4.54$ and $k = .0095$ inches

$p_t = 300$ cm Hg

$D_{\text{Body \& Nose}} = .0036 \times 300 = 1.08$ lbs

$D_{\text{Nose}} = .0026 \times 300 = \underline{.78}$ lbs

$\therefore D_{\text{Skin Friction}} = .30$ lbs

If $p_t = 140$, a minimum value at $M = 4.54$

$D_{\text{Body \& Nose}} = .55$ lbs

$D_{\text{Nose}} = \underline{.39}$ lbs

$\therefore D_{\text{Skin Friction}} = .16$ lbs

Now the JPL external, six-component balance has a low-scale drag range of ±20 lbs and at this range has an accuracy of about ±.02 lbs. It is clear from the above examples that at low Mach numbers and large k the accuracy is a fraction of one per cent, and that with increasing Mach number and decreasing roughness the accuracy becomes steadily worse until, in the worst case, the accuracy becomes about 10 per cent at $M = 4.54$ and $k \rightarrow 0$. For the majority of the data, it is estimated that the over-all accuracy is about 2 to 5 per cent. It is felt that this is quite adequate both for any practical engineering use of the results and also for numerical proof of the physical-aerodynamical conclusions to be drawn in a later section of this report.

It is interesting to look at figures 22 (JPL balance) and 25 (NOL balance) and notice that the internal consistency during a continuous wind-tunnel run is about an order of magnitude better than the accuracy from run to run, and this would be expected. The $k = 0$ values in figure 25 show the greatest scatter experienced from run to run under the most difficult conditions encountered; namely, maximum M and minimum k. The mean curve drawn through the k = 0 data is about 7 per cent below the data of Coles, which is certainly the most accurate data for smooth surfaces available.

B. Boundary-Layer Measurements

1. The JPL 12 x 12-inch supersonic wind tunnel. Velocity profile measurements were made in the turbulent boundary layer of a cone-cylinder model, the cylindrical portion of which was wrapped with sandpaper with sand grains of several sizes. The tests were conducted in the 12 x 12-inch supersonic wind tunnel of the Jet Propulsion Laboratory at the California Institute of Technology. This wind tunnel is continuous with a Mach-number range of about 1.3 to 4.0 and the Reynolds number is also variable. The jack-operated flexible-plate nozzle and test section with a model in place is shown in figure 32. The flow in the test section is very uniform, quantitatively the same as given in a previous section for the 18 x 20-inch tunnel.

2. Technique. The technique used for the boundary-layer-profile measurements is shown in the photograph of figure 33. The cone-cylinder model was mounted rigidly in the center of the tunnel parallel to the air stream. A small pitot tube was mounted on a vertical-traversing strut which can be hand cranked with a rack and pinion gear drive down through an opening in the ceiling of the test section. The internal opening of the pitot tube was rectangular with dimensions of 0.005 inches vertically and 0.012 inches laterally. Outside dimensions were 0.008 inches and 0.018 inches. The entrance of the pitot tube was fabricated from razor blade pieces.

A test run was made by cranking the pitot tube down in one direction, to remove the gear backlash, through the turbulent boundary layer until the pitot tube touched the surface of the model. Contact with the model surface, or top of the sand grains, was observed through the tunnel window optically using a Wild telescope level. This could be done with good accuracy since the flow, model and probe were all solid and stationary.

A typical schlieren photograph of the flow field and boundary-layer development along the model is shown in figure 34. Here again a wire ring at the nose of the model produced a turbulent boundary layer along the cylindrical portion of the model. The weak Mach lines emanating from the distributed roughness starting just downstream of the shoulder can be seen.

3. <u>Data reduction</u>. The measurements of u versus the distance y from the body are put into a nondimensional relationship in order to compare them with the corresponding incompressible results.

The relation is the "Prandtl Wall Velocity Law" for incompressible flows,

$$\frac{u}{v_*} = f\left(\frac{y\,v_*}{\nu}\,,\ \frac{y}{k}\right)\quad,\ y \longrightarrow 0 \tag{8}$$

for flow near the wall.

Now

$$\frac{y\,v_*}{\nu} = \frac{y\sqrt{\dfrac{\tau_w}{\rho_w}}}{\nu_w} = \frac{y\,V_1\sqrt{\dfrac{C_f}{2}}}{\nu_1\left(1+\dfrac{\gamma-1}{2}M_1^2\right)^{1.26}} \tag{9}$$

and was derived previously on page 12, equation 7.

Also

$$\frac{u}{v_*} = \frac{u}{\sqrt{\dfrac{\tau_w}{\rho_w}}} = \frac{u}{V_1}\cdot\frac{1}{\sqrt{\dfrac{C_f}{2}}\left(1+\dfrac{\gamma-1}{2}M_1^2\right)^{\frac{1}{2}}} \tag{10}$$

where the subscript 1 means values at the outer edge of the boundary layer where $y = \delta$.

The nondimensional ratios in Prandtl's relation above have thus been written in terms of the values of the variables at the wall for the compressible fluid.

A generalization of the incompressible-mixing-length theory to compressible flow by van Driest (ref. 12) shows that

$$\frac{u}{v_*} \text{ should be replaced by } \frac{\sin^{-1} m \dfrac{u}{u_1}}{\dfrac{m\sqrt{\tau_w/\rho_w}}{u_1}}$$

and $\dfrac{y\,v_*}{\nu}$ by $\dfrac{y\sqrt{\tau_w/\rho_w}}{\nu_w}$.

In the relation

$$\frac{\sin^{-1} m \dfrac{u}{u_1}}{\dfrac{m\sqrt{\tau_w/\rho_w}}{u_1}} = f\left(\frac{y\sqrt{\tau_w/\rho_w}}{\nu_w}\,,\ \frac{y}{k}\right), \qquad (11)$$

$$m^2 = \frac{(\gamma-1)\,M_1^2}{2 + (\gamma-1)\,M_1^2}$$

Equations 9, 10 and 11 permit the complete data reduction of the results of the boundary-layer measurements discussed in the next section.

4. Boundary-layer results. Boundary-layer measurements using the total head tube technique described above were made on a smooth model ($k = 0$) and models with sand-grain roughnesses of $k = 0.0027$, 0.0052 and

0.0131 inches average sand-grain diameter. The measurements were made at a station eight inches back of the nose, as shown in figure 33, at a free-stream Mach number $M_o = 2.60$ with a corresponding local surface Mach number $M_1 = 2.75$.

The raw data for the smooth model, k = 0, and the three rough ones are plotted in figures 35 to 38. The ratio of the total pressure measured by the pitot tube, p_t', to the supply pressure, p_{t_o}, is plotted against the height, h, of the center of the pitot tube above the surface of the model.

The velocity profiles obtained assuming constant total energy and constant static pressure through the boundary layer are shown in figures 39 and 40, where the ratio of the velocity u at a point y in the boundary layer to the velocity u_1 at the edge of the layer, $y = \delta$, is plotted against y and y/δ respectively.

The nondimensional velocity profiles are plotted in figure 41 in the form

$$\frac{\sin^{-1} m \frac{u}{u_1}}{\frac{m\sqrt{\tau_w/\rho_w}}{u_1}} \quad \text{vs} \quad \frac{y\sqrt{\tau_w/\rho_w}}{\nu_w} \qquad (12)$$

and in figure 42 in the form

$$\frac{u}{\sqrt{\frac{\tau_w}{\rho_w}}} \quad \text{vs} \quad \frac{y\sqrt{\tau_w/\rho_w}}{\nu_w} \qquad (13)$$

The smooth model data fit the incompressible logarithmic law for smooth surfaces

$$\frac{u}{v_*} = 5.5 + 5.75 \log \frac{yv_*}{\nu}$$

better when put in the form of equation 12 (fig. 41) than in the form of equation 13 (fig. 42).

It is seen that the effect of roughness is to displace the velocity profile downward essentially parallel to itself by an amount

$$\Delta \frac{\sin^{-1} m \frac{u}{u_1}}{\frac{m\sqrt{\tau_w/\rho_w}}{u_1}}$$

which is a function of the roughness Reynolds number $\frac{k\, v_*}{\nu}$.

When a surface is "fully rough," that is, the skin friction drag is quadratic, then Prandtl's Wall Law, equation 8, simplifies to

$$\frac{u}{v_*} = f_1\left(\frac{y}{k}\right), \quad y \rightarrow 0 \tag{14}$$

In the incompressible case, Nikuradse found this law to be (ref. 1)

$$\frac{u}{v_*} = 5.75 \log \frac{y}{k} + 8.5 \tag{15}$$

The velocity profiles of the present investigation are plotted in figure 43 in the form

$$\frac{\sin^{-1} m \frac{u}{u_1}}{\frac{m\sqrt{\tau_w/\rho_w}}{u_1}} \quad \text{vs} \quad \log \frac{y}{k}$$

and in figure 44 in the form

$$\frac{u}{\sqrt{\frac{\tau_w}{\rho_w}}} \quad \text{vs} \quad \log \frac{y}{k}$$

and in both cases Nikuradse's relation of equation 15 is included for comparison.

The downward displacement of the velocity profiles of figures 41 and 42 as a function of the roughness Reynolds number $\frac{k\,v_*}{\nu}$ is plotted in figure 45. It is clear that the quantitative shift in the velocity profile, whether defined as in figures 41 or 42, is remarkably close to the same as that obtained by Nikuradse in the incompressible case (ref. 1).

III. DISCUSSION AND INTERPRETATION OF THE RESULTS

The Skin Friction Drag Results

The skin friction drag results presented in figures 17 to 25 suggest the following observations:

The reliability of the experimental technique used in this investigation is demonstrated in figures 23 to 25 for supersonic speeds. It is shown in these figures that the measurements made with a smooth model are within 10 per cent of those obtained by Coles (ref. 8) by integrating carefully made local skin friction measurements to obtain the average skin friction coefficients. It has already been shown (p.16) that the combination of a smooth model and high Mach number produces the smallest drag forces and the largest errors. We may thus conclude that the measurements made with rough models with $k > .008$ inches are accurate to within about 5 per cent at least.

At the single subsonic Mach number, M = 0.70, at which tests were made the smooth model data coincide with the skin friction laws of von Kármán (ref. 14) and Coles (ref. 15) for M = 0 within the experimental error of the present test data (fig. 17). Now the measurements of Dhawan (ref. 16) show that at M = 0.70 the skin friction drag coefficient is about 3 per cent smaller than that of von Kármán for M = 0. Thus the present measurements at M = 0.70 are consistent with those of Dhawan at the same Mach number.

A comparison of the present data at M = 0.70 with those of Nikuradse at M = 0 (fig. 17) shows that for k = .024 inches and k = .038 inches the skin friction drag coefficient is in each case equal to about 89 per cent of Nikuradse's values at M = 0, and this compressibility effect is consistent with the supersonic compressibility effect for rough and smooth surfaces shown in figure 26. This general consistency between the present tests at M = 0.70, those of Dhawan at M = 0.70 for smooth surfaces, and those of Nikuradse at M = 0 for rough surfaces tends to confirm the correctness of the Prandtl-Schlichting-Nikuradse charts of reference 4 in a general way. The present data at M = 0.70 for k = .0095 inches coincide exactly with the Prandtl-Schlichting-Nikuradse data at M = 0 as shown in figure 17 for the same value of ℓ/k. Because all the JPL data correlate successfully at all values of k (fig. 31), it is concluded that the Prandtl-Schlichting-Nikuradse data for $\ell/k = 1680$ are about 10 per cent too small.

The compressibility effect for rough surfaces is shown in figure 26, and it is seen to be considerably greater than for smooth surfaces and to be essentially independent of the roughness size k.

The average skin friction drag coefficient results of the present investigation are summarized in figure 30 at a Reynolds number of 8×10^6 which is the maximum value attained.

In figure 31 the data of figure 30 are plotted as the ratio of the skin friction drag coefficient for the rough surface C_F to the value for the smooth surface C_{F_o} versus the logarithm of the "roughness" Reynolds number $\frac{kv_*}{\nu}$. The correlation is seen to hold for all Mach numbers up to about 5 and is the same functional relationship shown to hold in the incompressible case by Nikuradse (ref. 1). The important result follows that the Mach number is eliminated as a variable per se, and hence the effect of surface roughness on skin friction drag is localized deep within the boundary layer at the surface itself and is independent of the external flow. Now this result, that the roughness effect is universal and independent of the outside flow field, is precisely the assumption made by Prandtl and Schlichting in preparing their resistance charts of reference 4 for flat-plate boundary-layer flow from Nikuradse's data of reference 1 obtained from the flow of water inside circular pipes. The present results obviously strengthen this assumption as does the consistency of the subsonic data of the present investigation with that of Prandtl-Schlichting in figures 17 and 26 and the consistency of the subsonic and supersonic data of figure 31.

The Critical Roughness Size

A further important result is obtained from the correlation of figure 31. It is that the critical "roughness" Reynolds number below which the skin friction drag of a rough surface is the same as that of a smooth surface is

$$\frac{k_c v_*}{\nu} \cong 10 \text{ for all M up to about 5.}$$

Hence if $k < \frac{10\,\nu}{v_*}$, then the surface is hydraulically smooth. k_c is the critical roughness size. The practical importance of this result is obvious.

It is interesting to note that the above value of the critical roughness size $k_c \cong \frac{10\,\nu}{v_*}$ is numerically the same as the thickness of the laminar sublayer of the turbulent boundary layer on a smooth surface at both subsonic and supersonic speeds.

Now, since the surface is hydraulically smooth if k is less than the laminar sublayer height of a physically smooth surface, one is led back to the simple idea suggested many years ago, that the mechanism of the drag increase due to roughness of the sand-grain type is that below the critical roughness size the flow about the roughness element is laminar. As the roughness size increases a point is reached where vortices are formed behind the roughness element, turbulent flow about the roughness element ensues and the drag rises steadily according to the quadratic law as the roughness size is increased further. Clearly, then one is interested in the critical Reynolds number based on the roughness size and the local velocity at the top of the roughness element.

It is easy to show that if

$$k_c \cong \frac{10\,\nu}{v_*}\;, \qquad \text{then} \quad \frac{k_c u_k}{\nu} = \frac{10}{\sqrt{\frac{C_f}{2}}} \cdot \frac{u_k}{V}$$

u_k = velocity at $y = k$

y = height above a smooth surface.

V = velocity at the edge of the boundary layer.

Since k_c is about equal to the laminar sublayer height for a smooth surface, u_k is the velocity at the edge of the laminar sublayer.

In order to make an estimate of $\frac{k_c u_k}{\nu}$, $\frac{u_k}{V}$ for a turbulent boundary layer at an average Mach number of 3 is about .65 and C_f is about .0015 at $R = 8 \times 10^6$.

$$\therefore \quad \frac{k_c u_k}{\nu} = 250$$

In a very interesting investigation of the effect of a sandpaper roughness on boundary-layer transition at low speeds, von Doenhoff and Horton (ref. 17) found that turbulent spots occurred in the laminar flow at the roughness when $\frac{k\, u_k}{\nu} = 320$, and furthermore this value was critical. That is, if $\frac{k\, u_k}{\nu}$ was just slightly less than 320 the flow in the boundary layer was completely laminar. The extent of the area covered with sand grains in the stream direction did not have any important effect on the critical value of the roughness Reynolds number.

It appears reasonable to conclude from the above discussion that the mechanisms of the drag rise due to sand-grain roughness in turbulent flow at the critical roughness Reynolds number and of the critical occurrence of transition in the laminar boundary layer on a sand-grain-roughened surface are probably the same, and that the mechanism is simply the breakdown of local laminar flow about the sand-grain roughness element to form turbulent flow at a critical roughness Reynolds number.

The Velocity Profiles

The velocity profile results have been discussed already when they were presented in the previous section.

It remains to observe that the turbulent velocity profile for the smooth surface at supersonic speeds follows the Prandtl Wall Law

$$\frac{u}{v_*} = f\ (\log \frac{yv_*}{\nu})$$

in its logarithmic portion (fig. 41).

When the surface is "fully rough," that is the skin friction drag is quadratic, the velocity profiles then follow the Prandtl Wall Law

$$\frac{u}{v_*} = f\ (\log \frac{y}{k})$$

in their logarithmic portion (fig. 43).

The displacement $\triangle \frac{u}{v_*}$ of the velocity profiles of figure 41 with increasing roughness size k is shown in figure 45 to be a function only of the roughness Reynolds number $\frac{kv_*}{\nu}$. It is clear furthermore that the present data at $M_1 = 2.75$ check exactly with the low-speed data of Nikuradse (ref. 1). Since the displacement $\triangle \frac{u}{v_*}$ of the velocity profile is proportional to the drag increase due to roughness and since the drag increase due to roughness is a function only of the roughness Reynolds number (fig. 31), it is clear that the exact check between the compressible and incompressible velocity profile shifts shown in figure 45 must follow. Finally then, the drag correlation of figure 31 and the velocity profile correlation of figure 45 taken together completely unify the subsonic and supersonic skin friction drag measurements of the present investigation and the incompressible skin friction drag measurements of Nikuradse (refs. 1 and 4).

IV. CONCLUSIONS

The following conclusions can be drawn from the present investigation:

1. At subsonic and supersonic speeds up to a Mach number of 5, and for roughness sizes such that the quadratic resistance law holds, the compressibility effect is indirect and the skin friction drag is a function only of the roughness Reynolds number $\frac{kv_*}{\nu}$, just as in the incompressible case.

2. The critical roughness below which the surface is hydraulically smooth is $k_{critical} \cong \frac{10\,\nu}{v_*}$ independent of Mach number, and this is equal to the thickness of the laminar sublayer for a smooth surface for both compressible and incompressible flows.

3. Over the range of roughness sizes considered here there appears to be no wave drag associated with the drag due to roughness.

4. The shift in the turbulent velocity profile $\Delta \frac{u}{v_*}$ for a rough surface at supersonic speeds is a function only of the roughness Reynolds number $\frac{kv_*}{\nu}$ and quantitatively follows identically the same law as in the incompressible case.

Two suggestions for further research in this field present themselves:

1. It would be very desirable to carry out measurements of the skin friction drag of rough surfaces at M = 0 in order to compare them with

the present results and with those of Nikuradse obtained from pipe flow. This will probably be accomplished by the present program believed to be under way at Göttingen and alluded to in the Introduction.

2. It would be very interesting to survey the detailed flow structure over a sand-grain rough surface blown up in scale to a size such that the flow details can be physically observed at the critical roughness Reynolds number in order to completely understand the mechanism behind the grossly observed effects of roughness on skin friction drag and on the boundary-layer velocity profile.

V. REFERENCES

1. Nikuradse, J., "Strömungsgesetze in rauhen Rohren," <u>V. D. I. Forschungsheft</u>, (1933), No. 361. (English Translation, <u>Laws of Flow in Rough Pipes</u>, NACA Technical Memorandum 1292, (1950).)

2. Hama, F. R., "Boundary Layer Characteristics for Smooth and Rough Surfaces," <u>Transactions of the Society of Naval Architects and Marine Engineers</u>, (1954), Vol. 62, pp. 333-358.

3. Clauser, F. H., "The Turbulent Boundary Layer," <u>Advances in Applied Mechanics</u>, (1956), Vol. IV, Academic Press Inc., New York, N. Y., 413 pp.

4. Prandtl, L. and Schlichting, H., "Das Widerstandsgesetz rauher Platten," <u>Werft, Reederei und Hafen</u>, (1934), Jahrg. 15, Heft 1. (An account in English is given in Durand, <u>Aerodynamic Theory</u>, (1936), Vol. III.)

5. Wade, J. H. T., <u>An Experimental Investigation of the Effect of Surface Roughness on the Drag of a Cone-Cylinder Model at a Mach Number of 2.48</u>, UTIA Report No. 34, (1955), Institute of Aerophysics, University of Toronto.

6. Chapman, D. R. and Kester, R. H., "Measurements of Turbulent Skin Friction on Cylinders in Axial Flow at Subsonic and Supersonic Velocities," <u>Journal of the Aeronautical Sciences</u>, (1953), Vol. 20, No. 7, pp. 441-448.

7. Wilson, R. E., "Turbulent Boundary Layer Growth with Favorable Static Pressure Gradient at Supersonic Speeds," Proceedings of the Second Midwestern Conference on Fluid Mechanics, (1952), The Ohio State University, Columbus, Ohio.

8. Coles, D., Measurements in the Boundary Layer on a Smooth Flat Plate in Supersonic Flow. III. Measurements in a Flat-Plate Boundary Layer at the Jet Propulsion Laboratory, JPL Report No. 20-71, (1953); and "Measurements of Turbulent Friction on a Smooth Flat Plate in Supersonic Flow," Journal of the Aeronautical Sciences, (1954), Vol. 21, No. 7, pp. 433-448.

9. Jakob, M. and Dow, W. M., "Heat Transfer from a Cylindrical Surface to Air in Parallel Flow with and without Unheated Starting Sections," Transactions of the American Society of Mechanical Engineers, (1946), Vol. 68, No. 2, pp. 123-134.

10. Eckert, H. V., "Simplified Treatment of the Turbulent Boundary Layer Along a Cylinder in Compressible Flow," Journal of the Aeronautical Sciences, (1952), Vol. 19, No. 1, p. 23.

11. von Kármán, T., "The Problem of Resistance in Compressible Fluids," V Convegno della Fondazione Alessandro Volta, (1935), Reale Accademia d'Italia, Rome, pp. 226-290.

12. van Driest, E. R., "Turbulent Boundary Layer in Compressible Fluids," Journal of the Aeronautical Sciences, (1951), Vol. 18, No. 3, pp. 145-160.

13. Kendall, J. M., Precision Drag Balance of One Component, NAVORD Report No. 2420, (1952), U. S. Naval Ordnance Laboratory, White Oak, Maryland, 13 pp.

14. Schoenherr, Karl E., "Resistance of Flat Surfaces Moving Through a Fluid," Transactions of the Society of Naval Architects and Marine Engineers, (1932), Vol. 40.

15. Coles, Donald, "The Problem of the Turbulent Boundary Layer," Journal of Applied Mathematics and Physics (Zeitschrift für angewandte Mathematik und Physik), (1954), Vol. V, Fasc. 3, pp. 181-203.

16. Dhawan, Satish, Direct Measurements of Skin Friction, NACA Report No. 1121, (1953), 20 pp.

17. von Doenhoff, Albert E. and Horton, Elmer A., A Low-Speed Experimental Investigation of the Effect of a Sandpaper Type of Roughness on Boundary-Layer Transition, NACA Technical Note No. 3858, (1956), 43 pp.

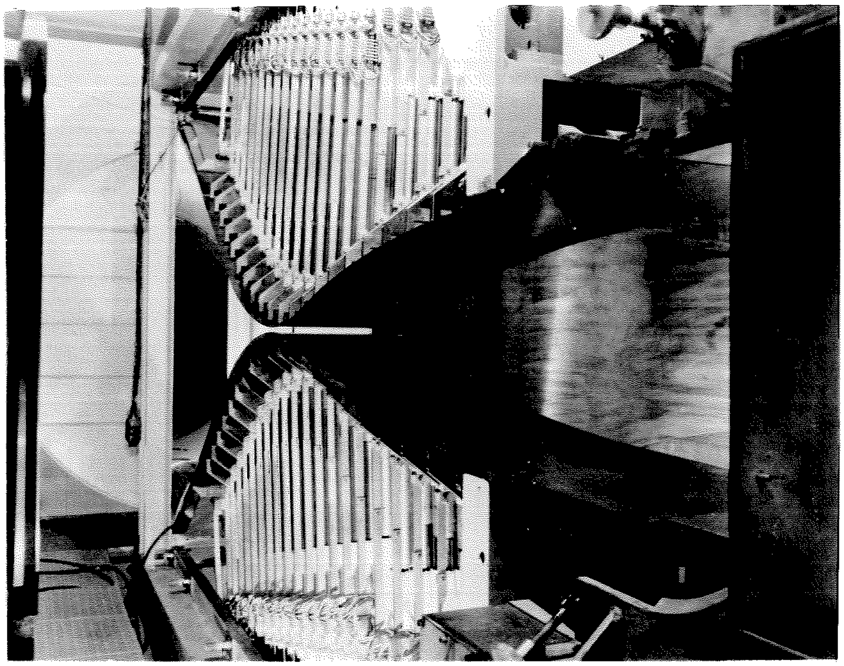

Figure 1. The JPL 18 × 20-Inch Supersonic Wind Tunnel

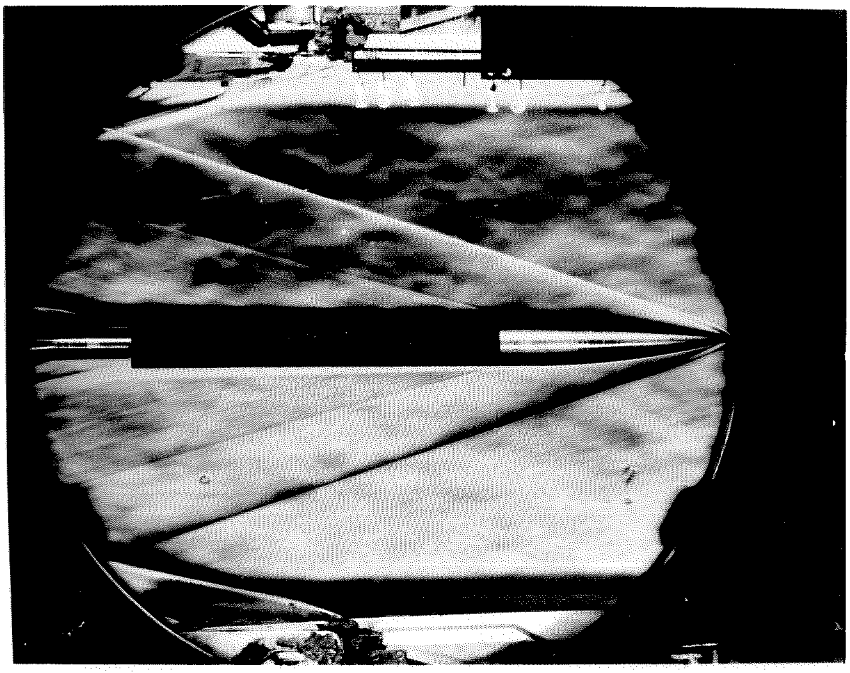

Figure 2. Typical Model Installation

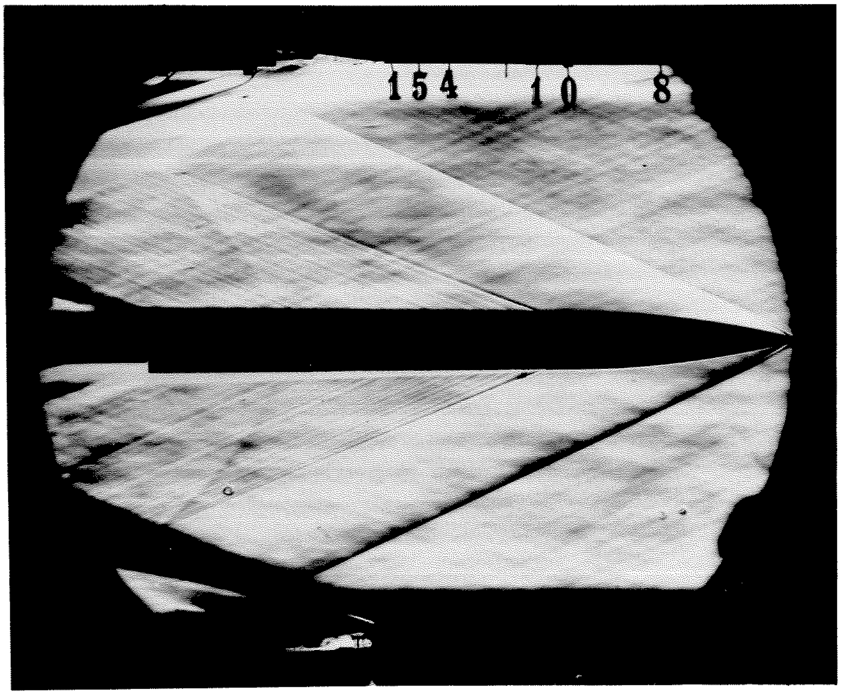

Figure 3. Schlieren Photograph of the Complete Model – M = 2.56

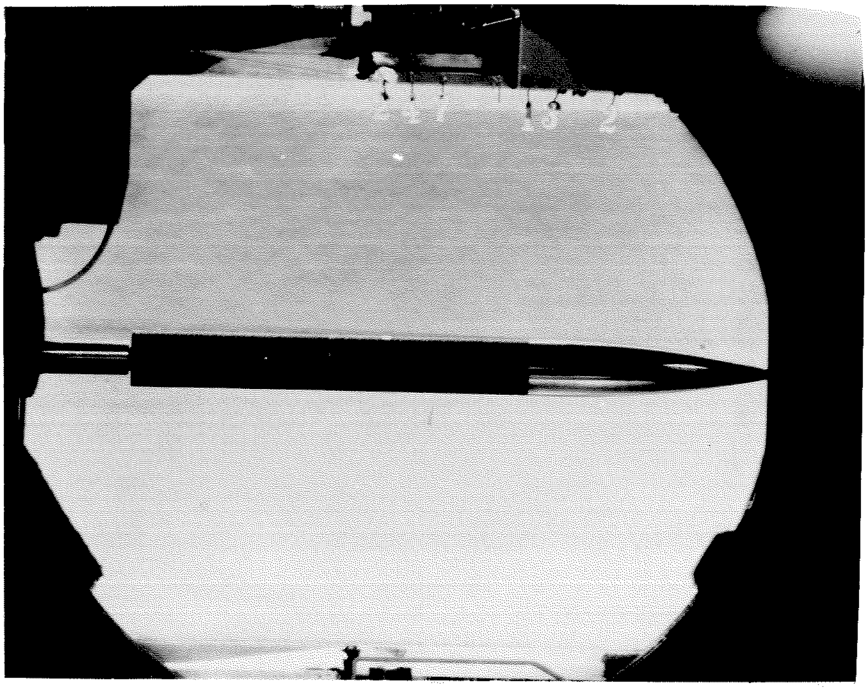

Figure 3a. Schlieren Photograph of the Complete Model – M = 0.70

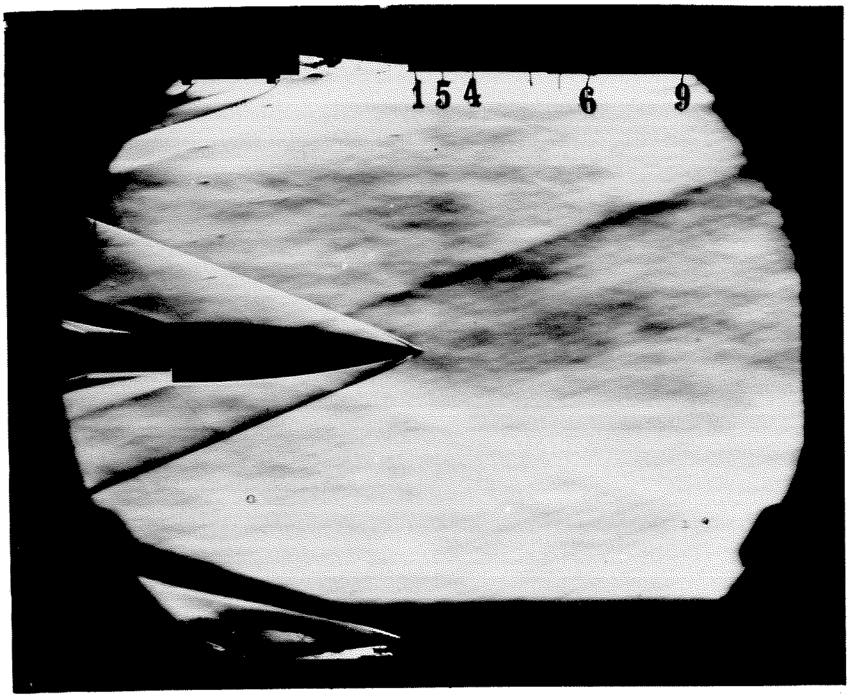

Figure 4. Schlieren Photograph of the Ogival Nose – M = 3.07

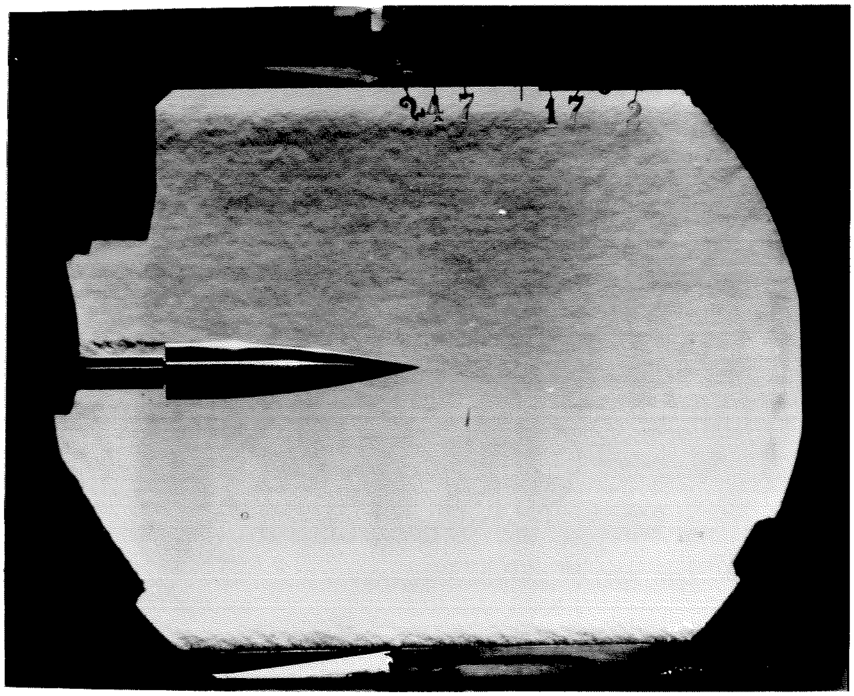

Figure 4a. Schlieren Photograph of the Ogival Nose – M = 0.70

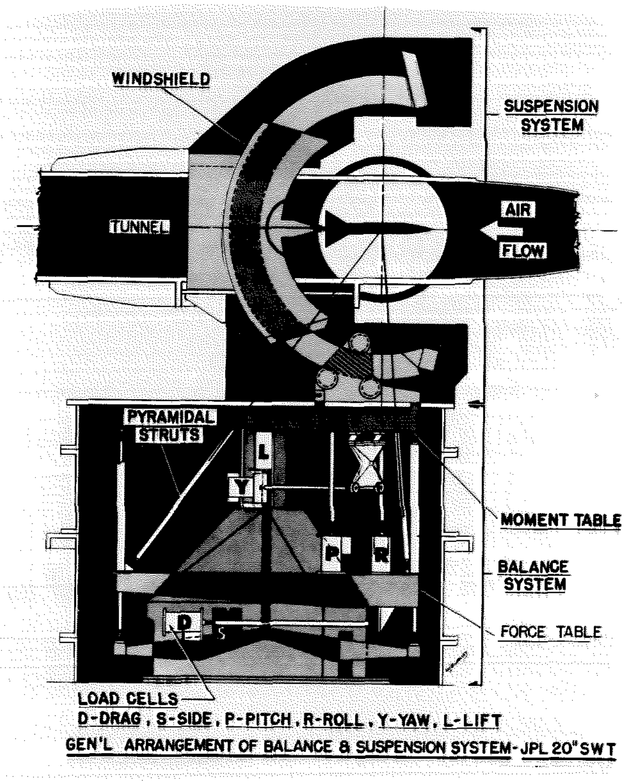

Figure 5. Balance and Suspension System of the 18 × 20-Inch Supersonic Wind Tunnel – Schematic

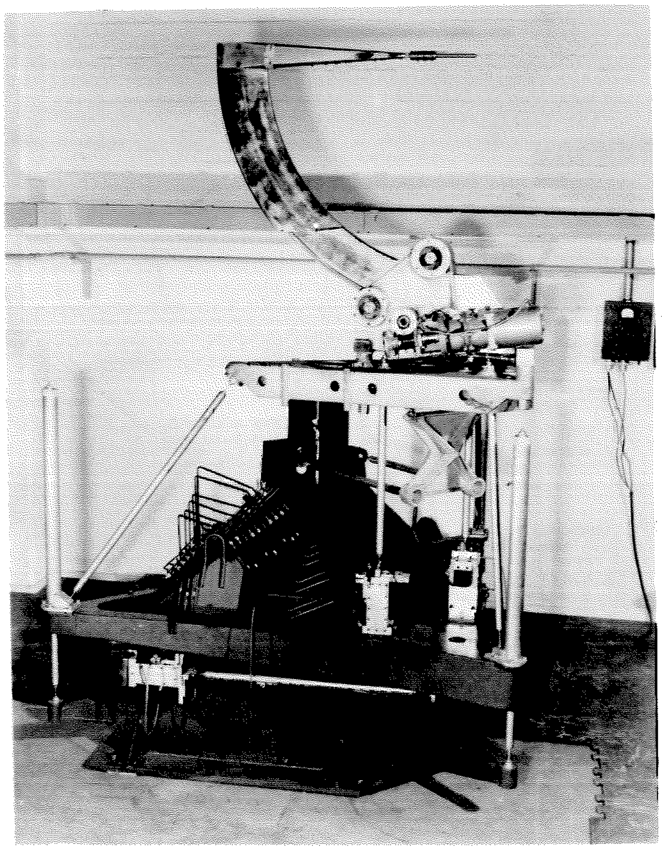

Figure 6. Balance and Suspension System of the 18 × 20-Inch Supersonic Wind Tunnel – Photograph

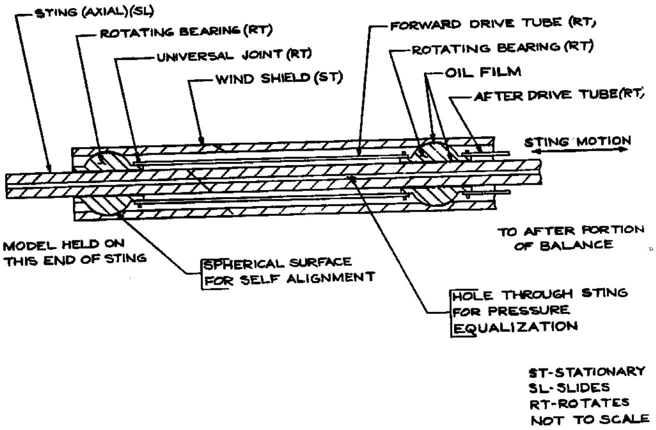

Figure 7. The NOL Drag Balance – Forward End – Schematic

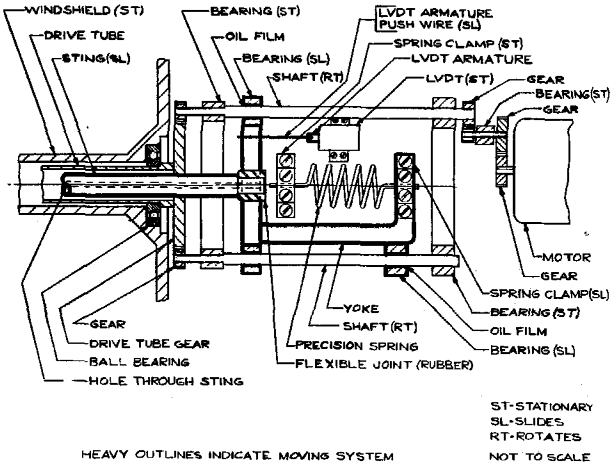

Figure 7a. The NOL Drag Balance – Aft End – Schematic

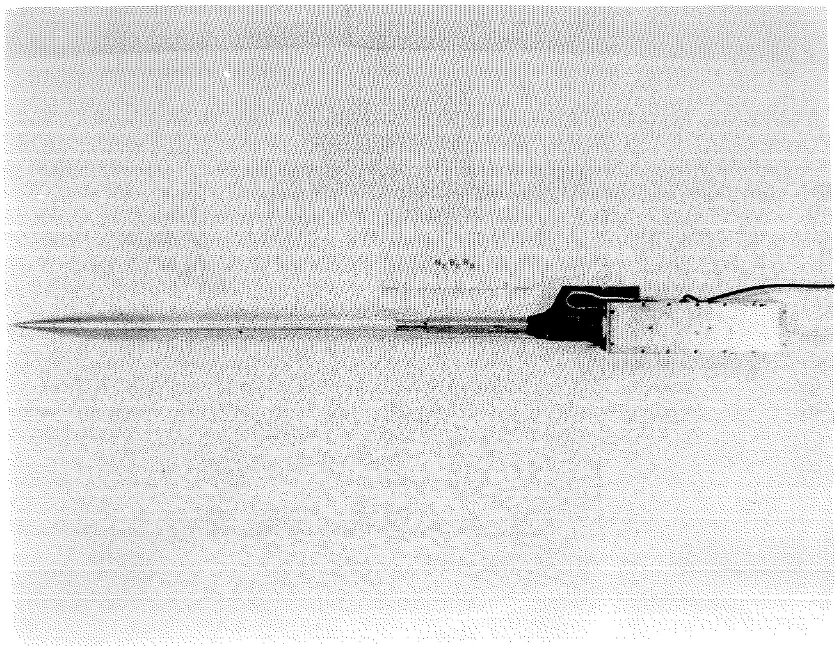

Figure 8. The NOL Drag Balance and Model

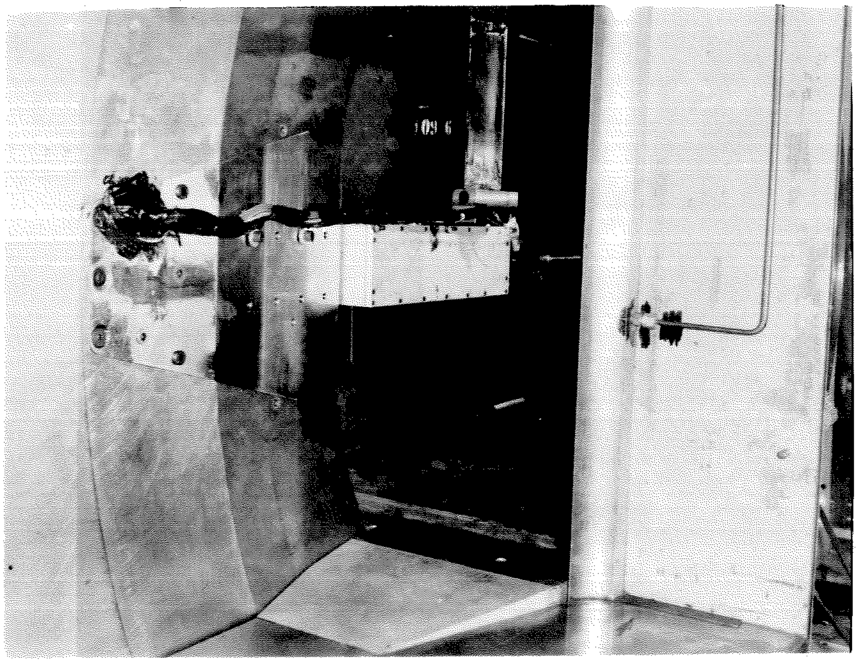

Figure 9. The NOL Drag Balance Installed in the Tunnel

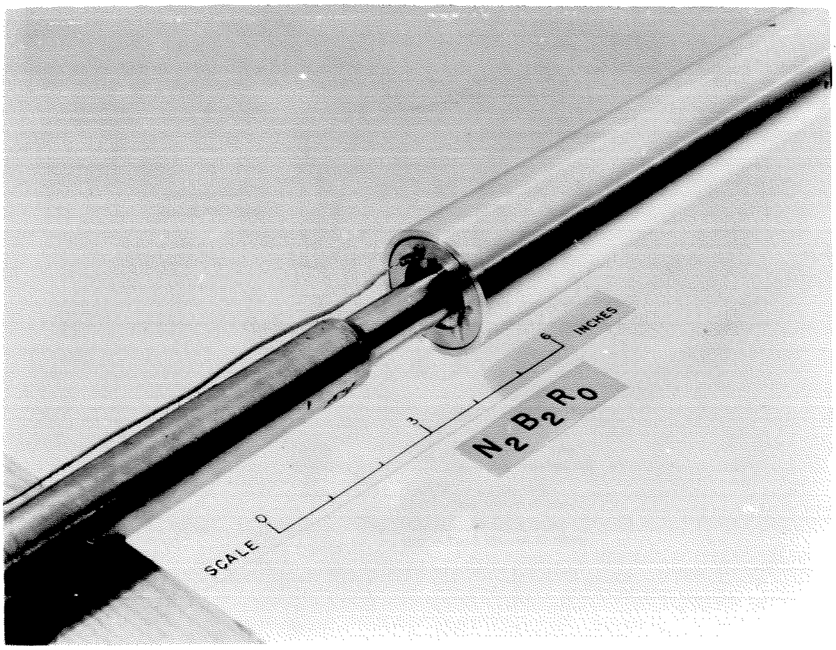

Figure 10. Sting-Model Connection and Base Pressure Annulus

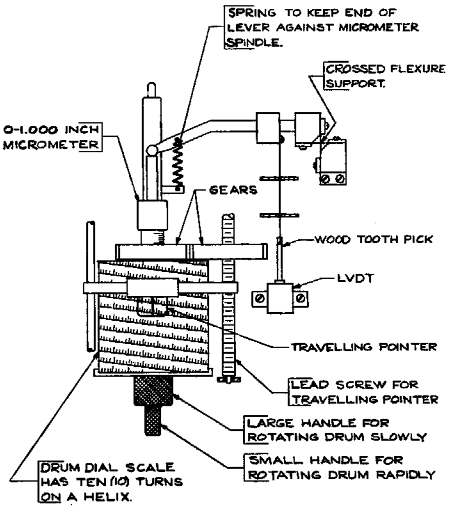

Figure 11. Schematic Diagram of the Reader

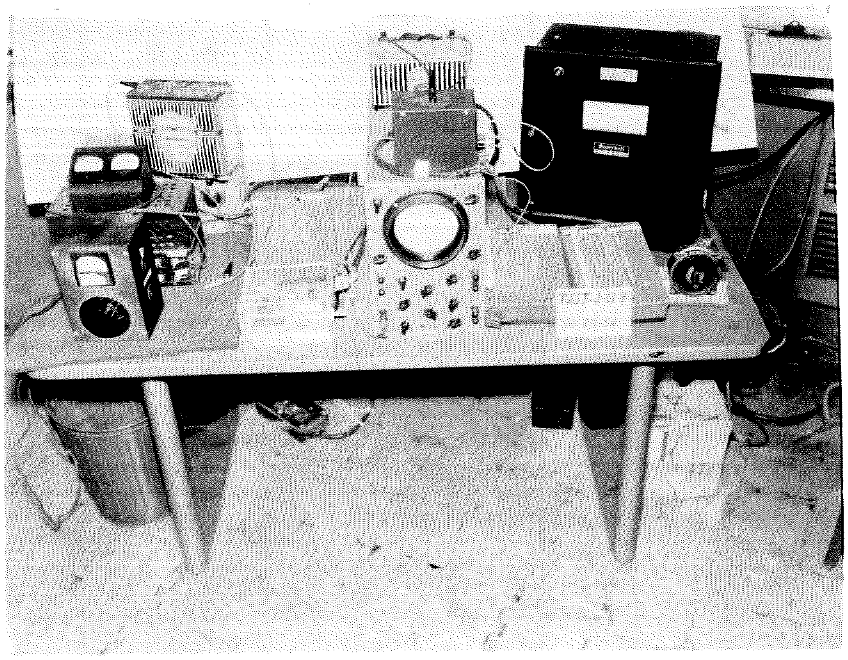

Figure 12. Reader Box and Associated Electrical Equipment

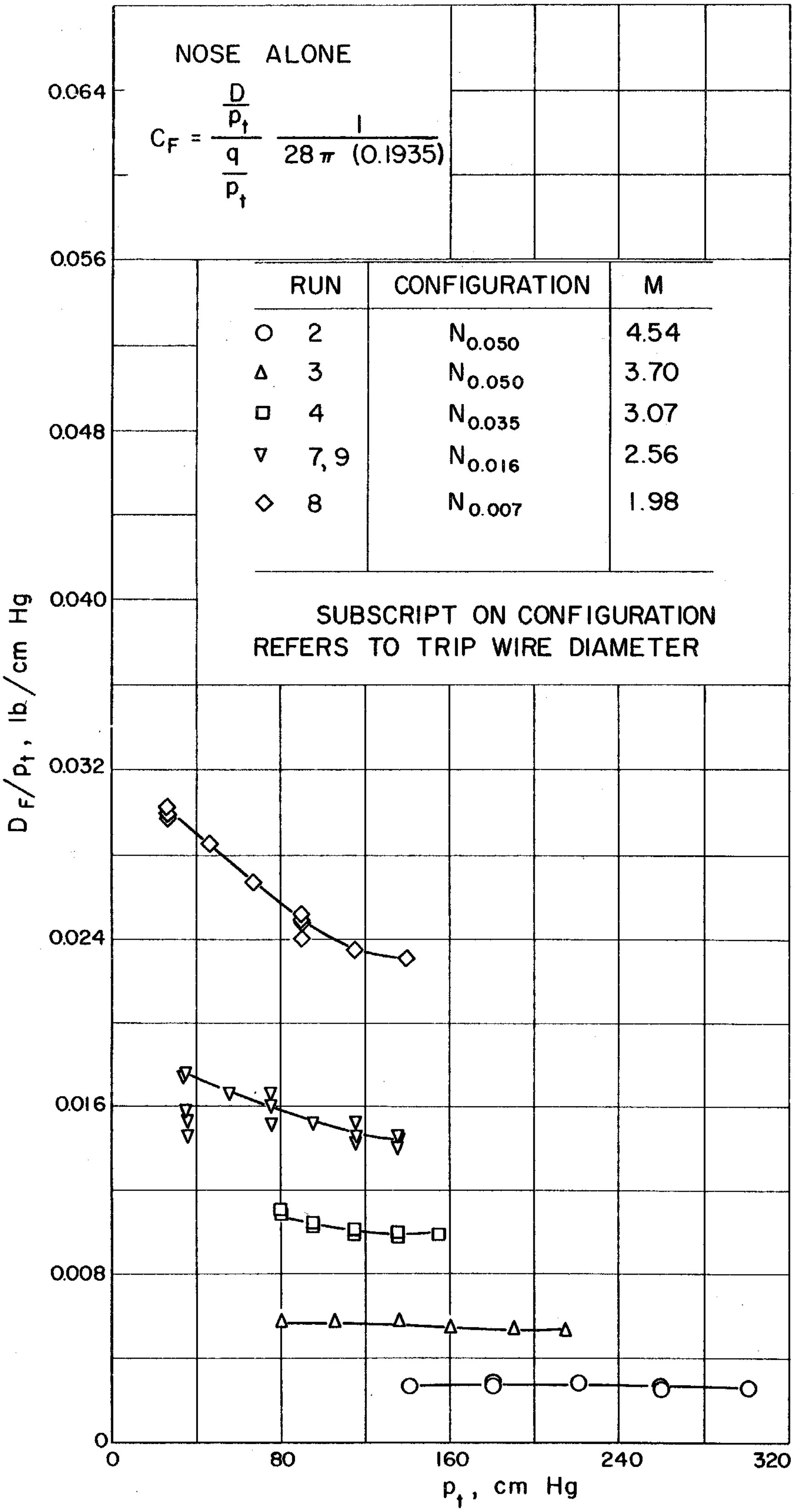

Figure 13. Fore Drag - Nose Alone

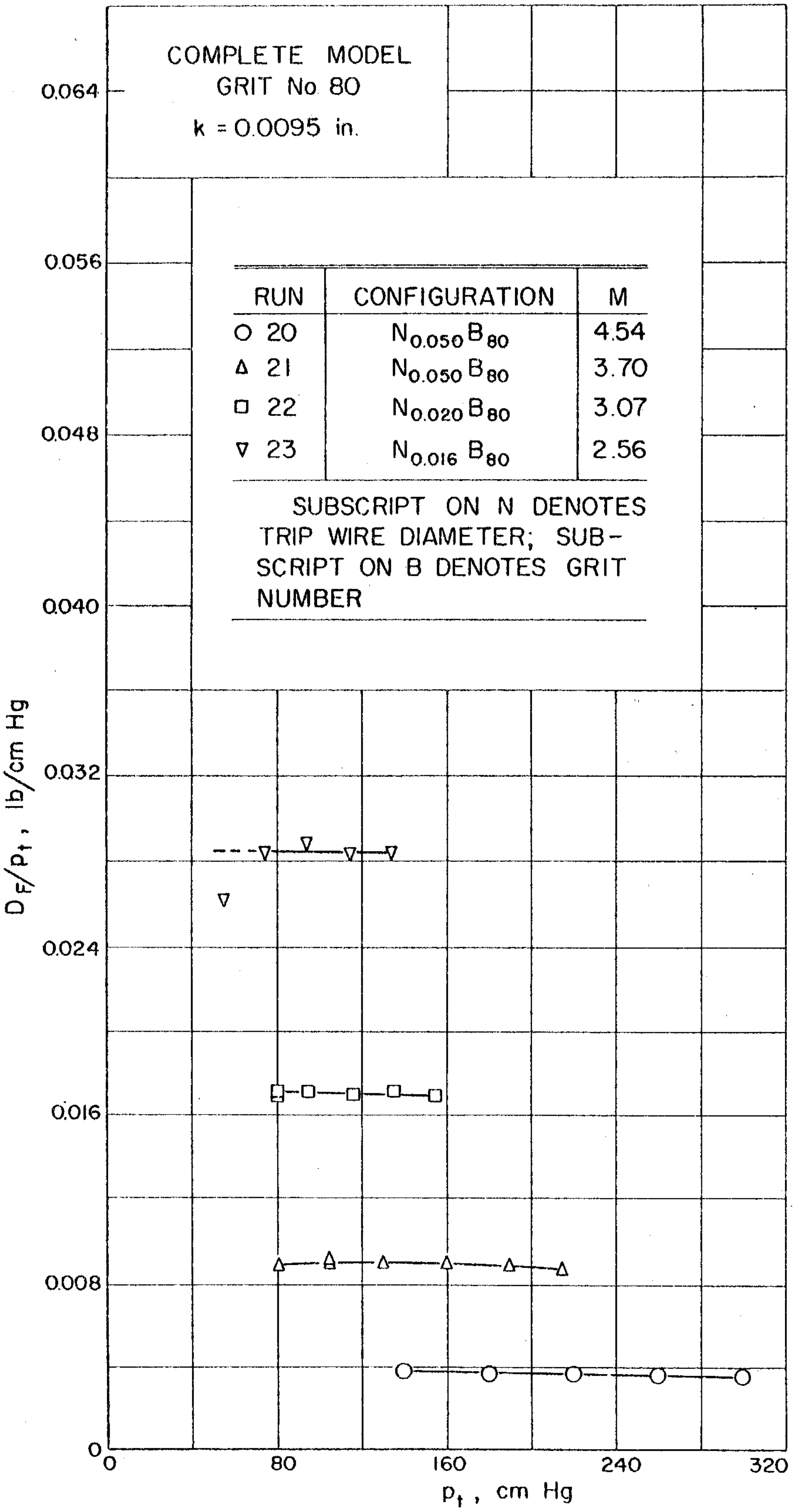

Figure 14. Fore Drag - Complete Model (k = .0095 in.)

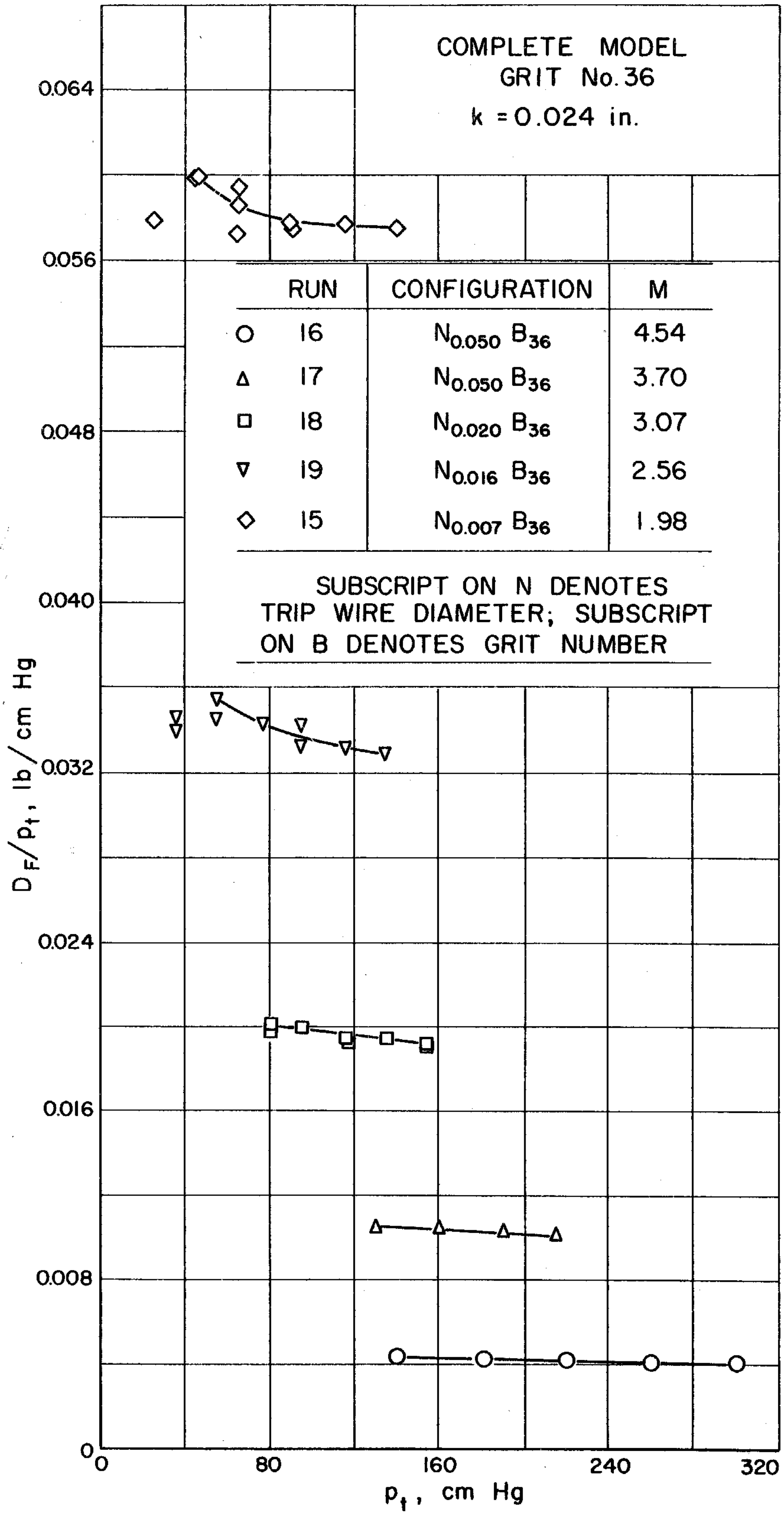

Figure 15. Fore Drag - Complete Model (k = .024 in.)

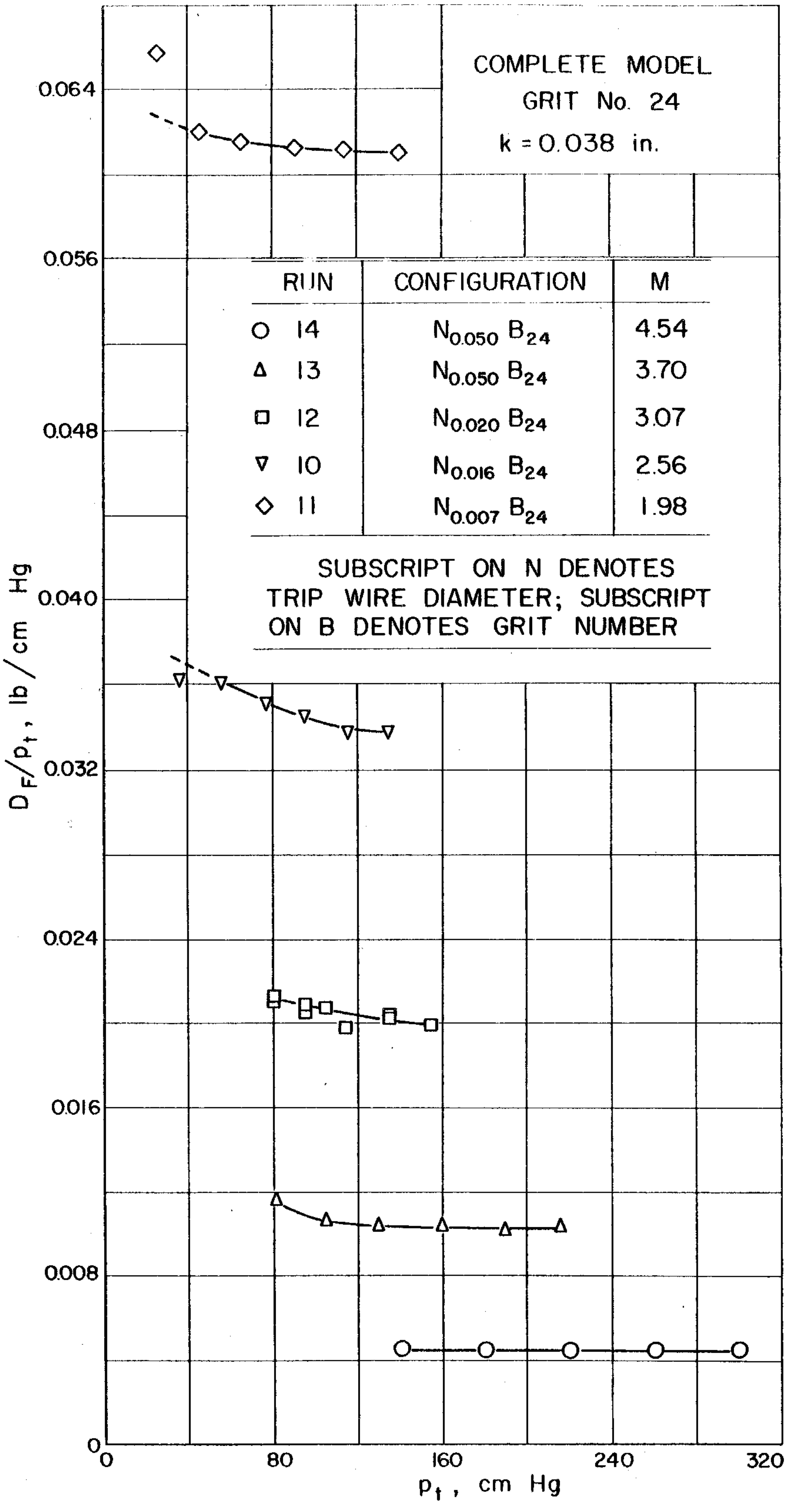

Figure 16. Fore Drag - Complete Model (k = .038 in.)

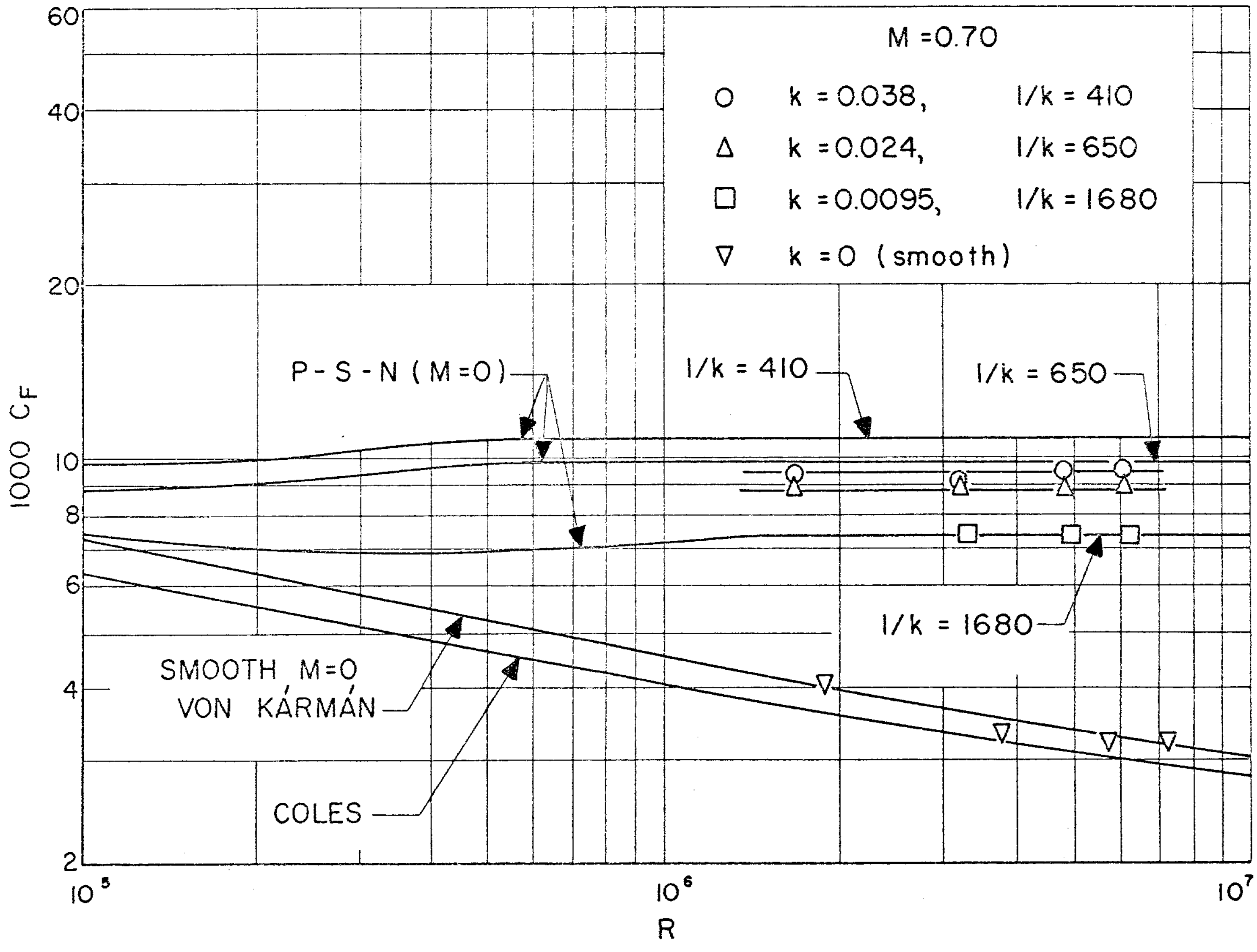

Figure 17. Average Skin Friction Drag Coefficient vs Reynolds Number - M = 0.70

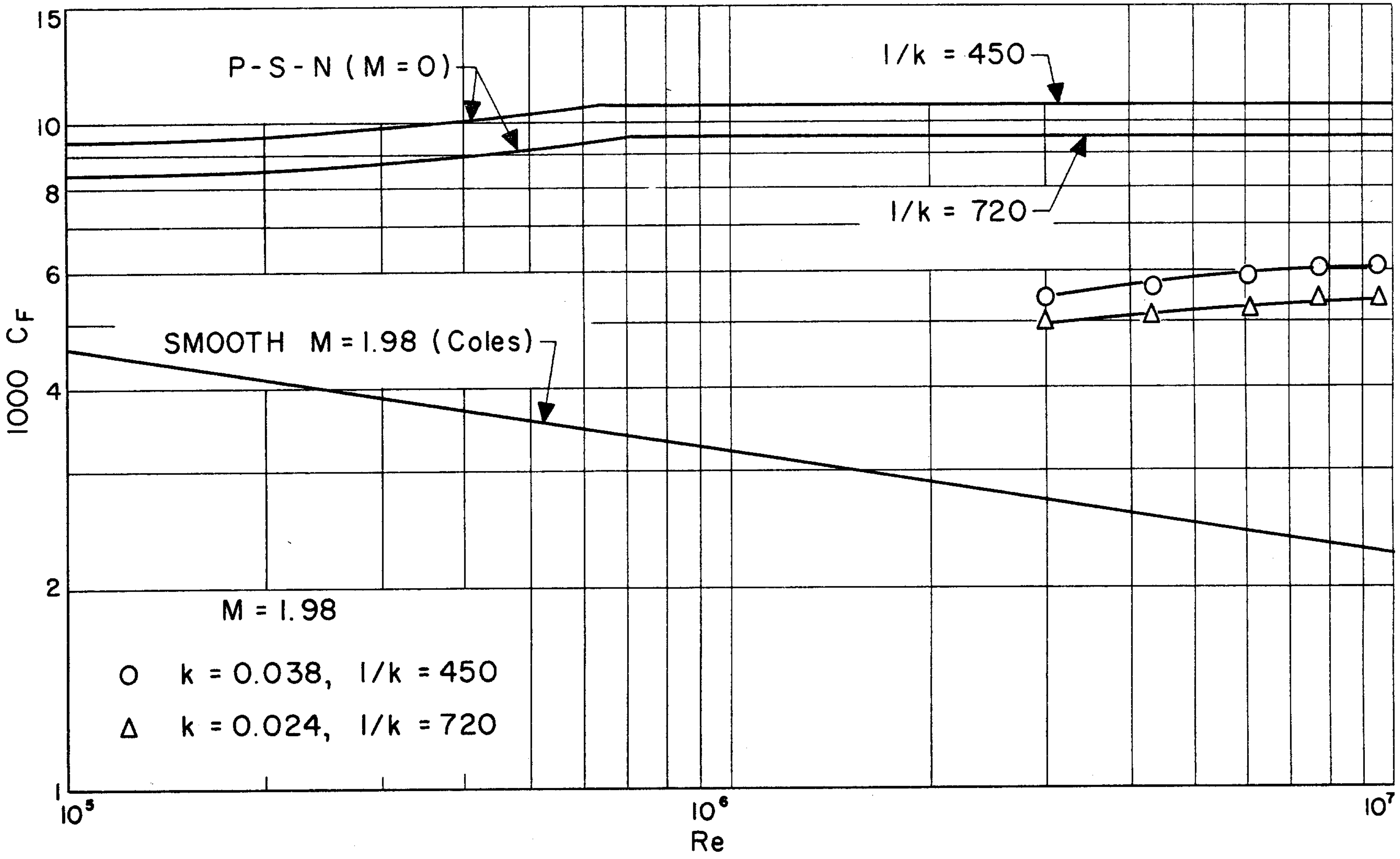

Figure 18. Average Skin Friction Drag Coefficient vs Reynolds Number - M = 1.98

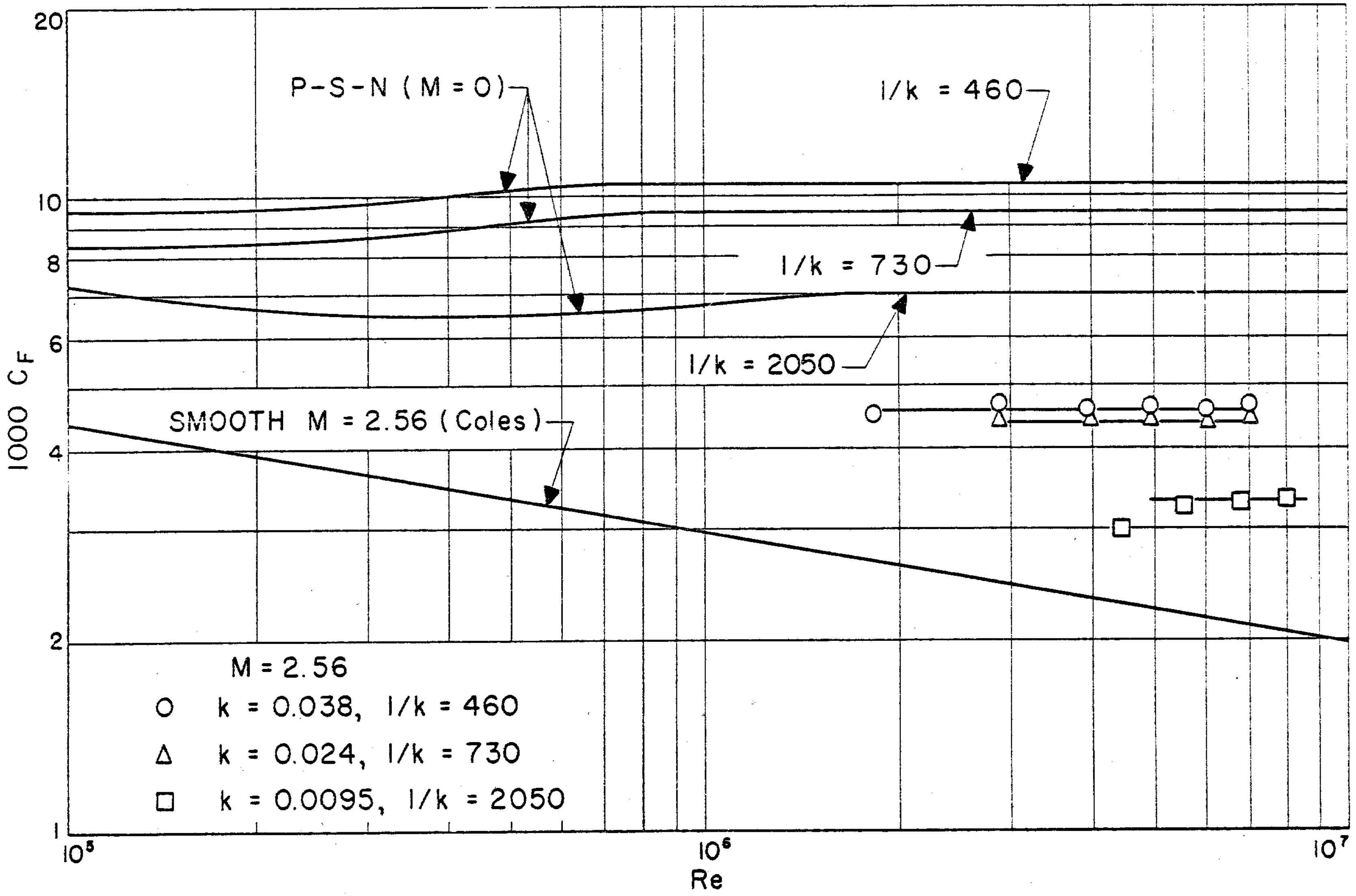

Figure 19. Average Skin Friction Drag Coefficient vs Reynolds Number - M = 2.56

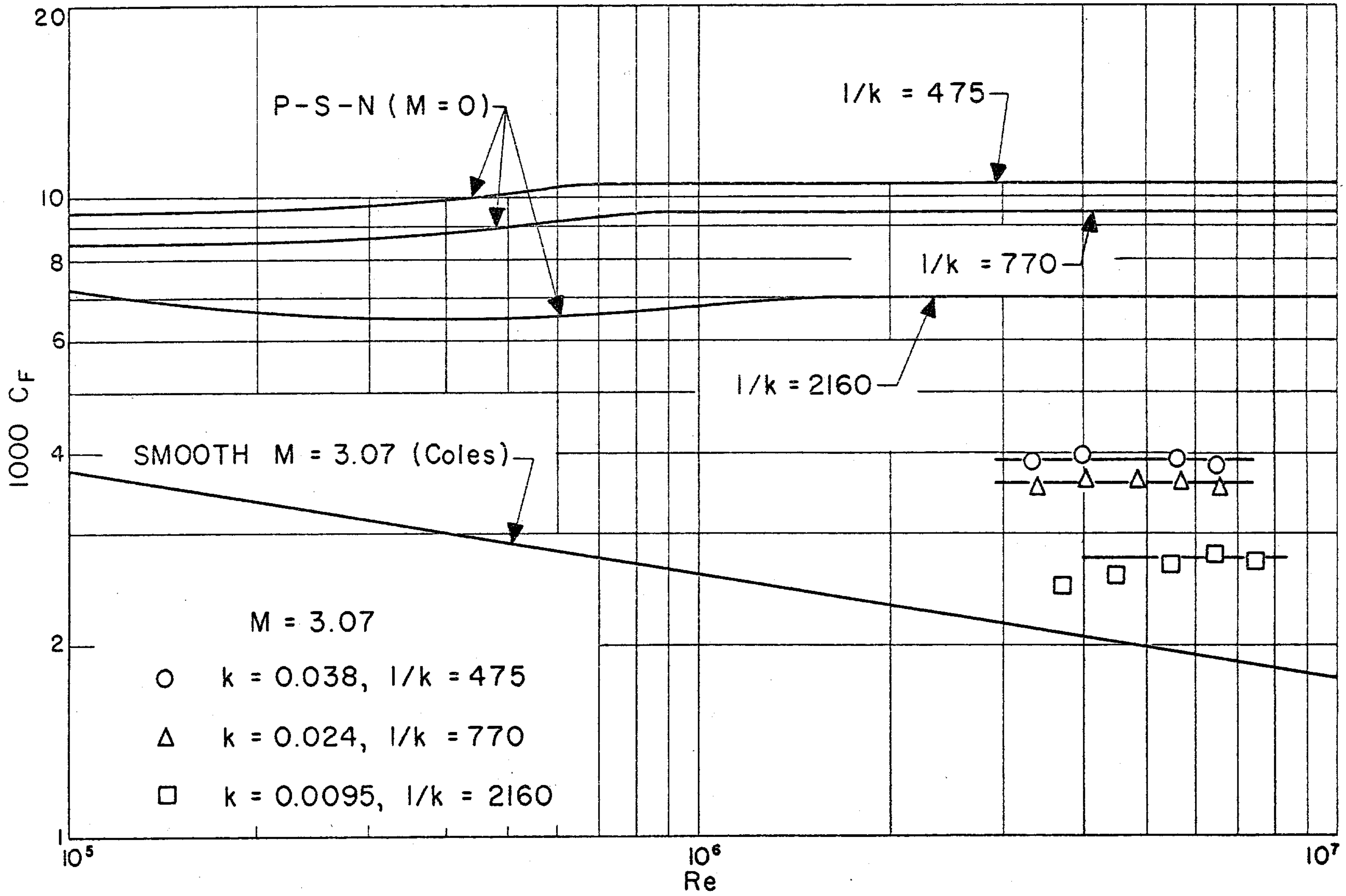

Figure 20. Average Skin Friction Drag Coefficient vs Reynolds Number - M = 3.07

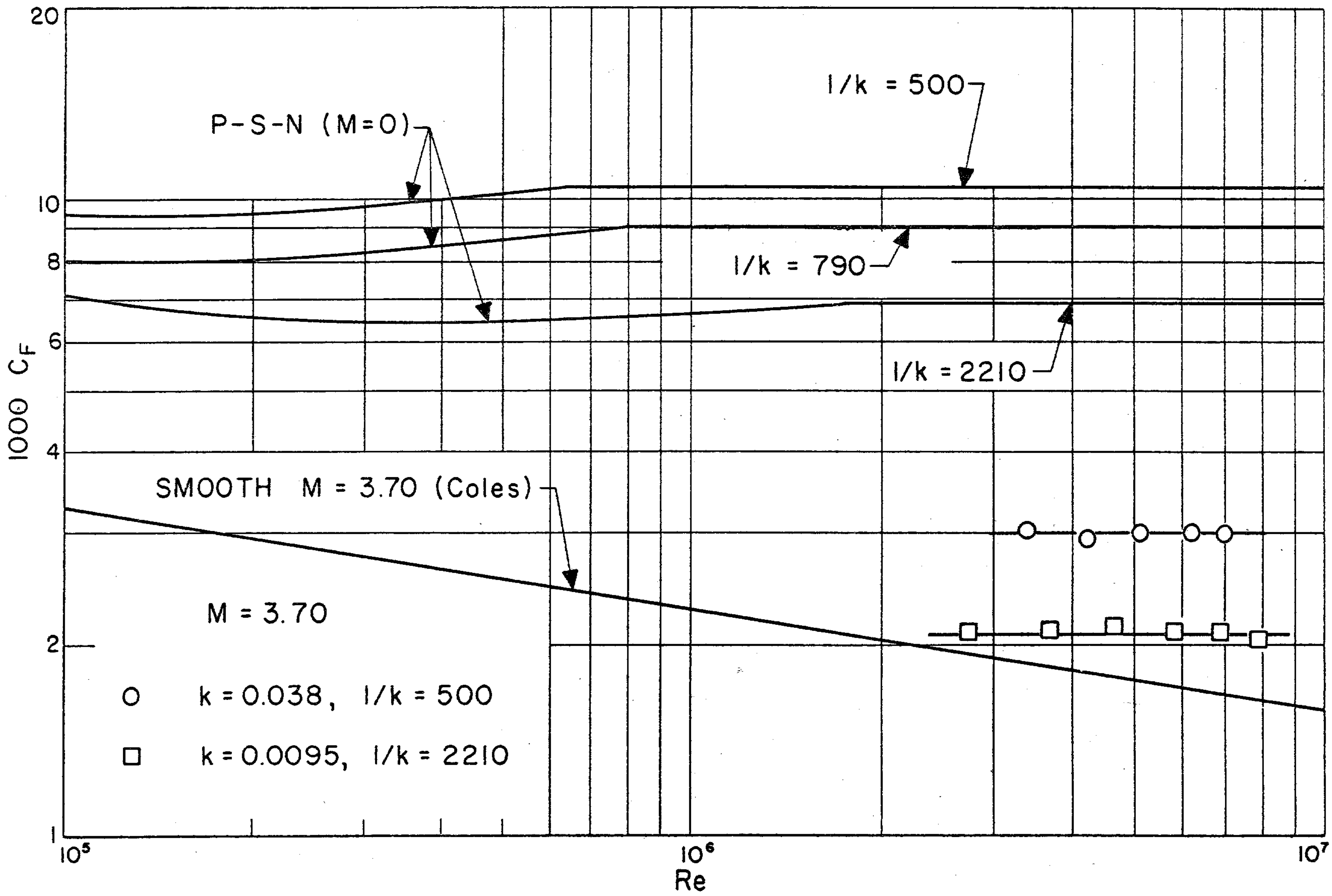

Figure 21. Average Skin Friction Drag Coefficient vs Reynolds Number - M = 3.70

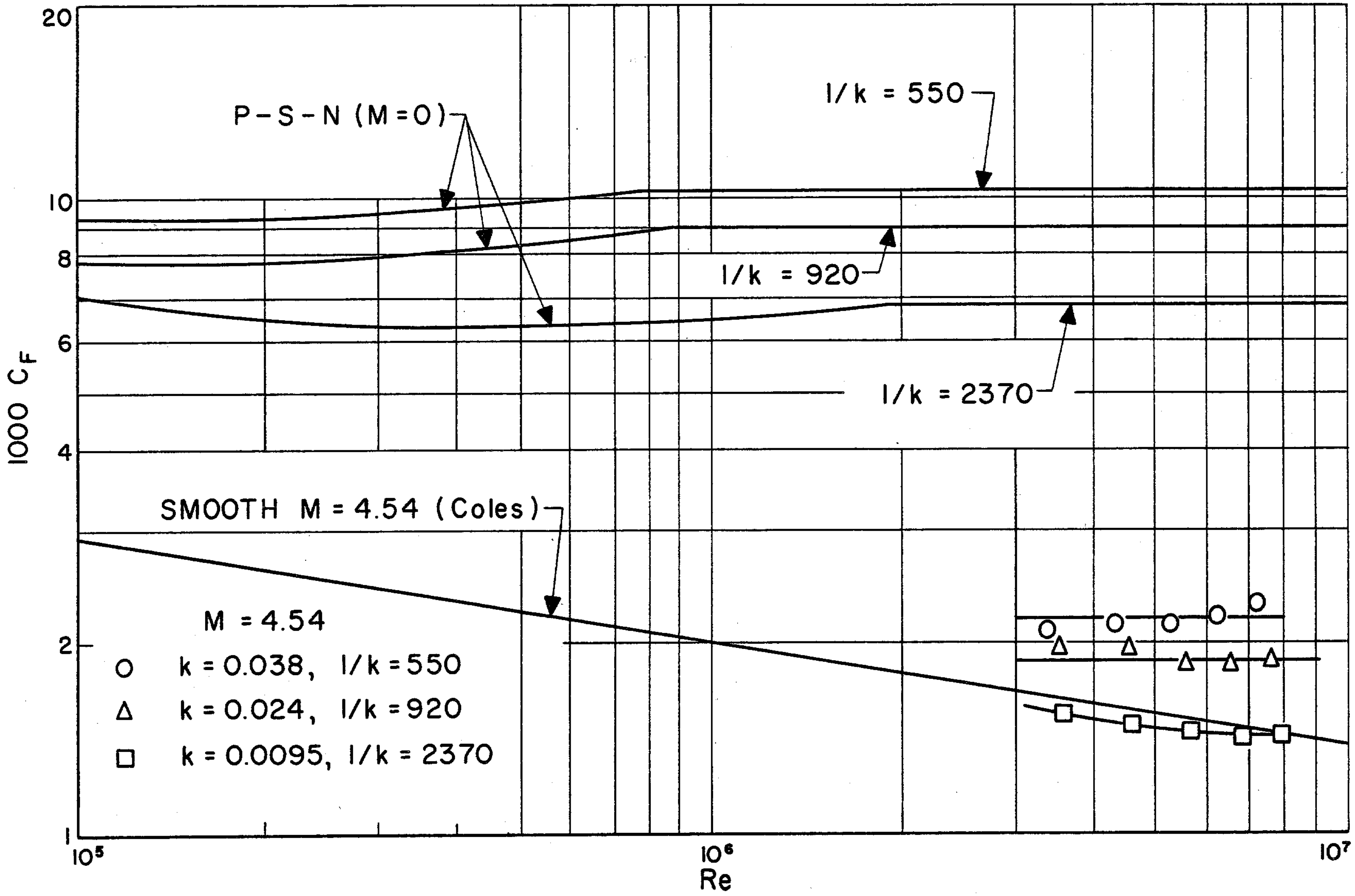

Figure 22. Average Skin Friction Drag Coefficient vs Reynolds Number - M = 4.54

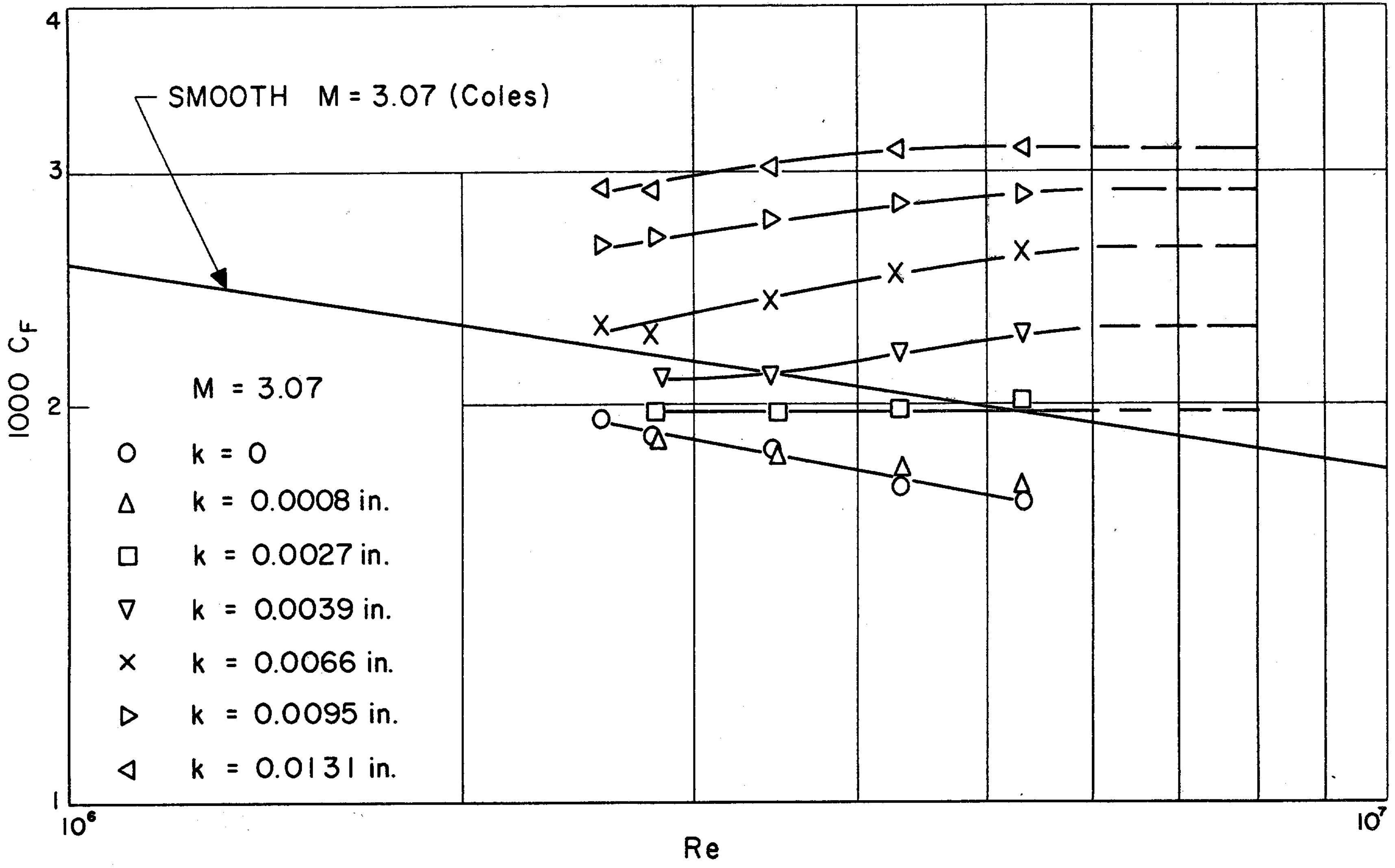

Figure 23. Average Skin Friction Drag Coefficient vs Reynolds Number - M = 3.07

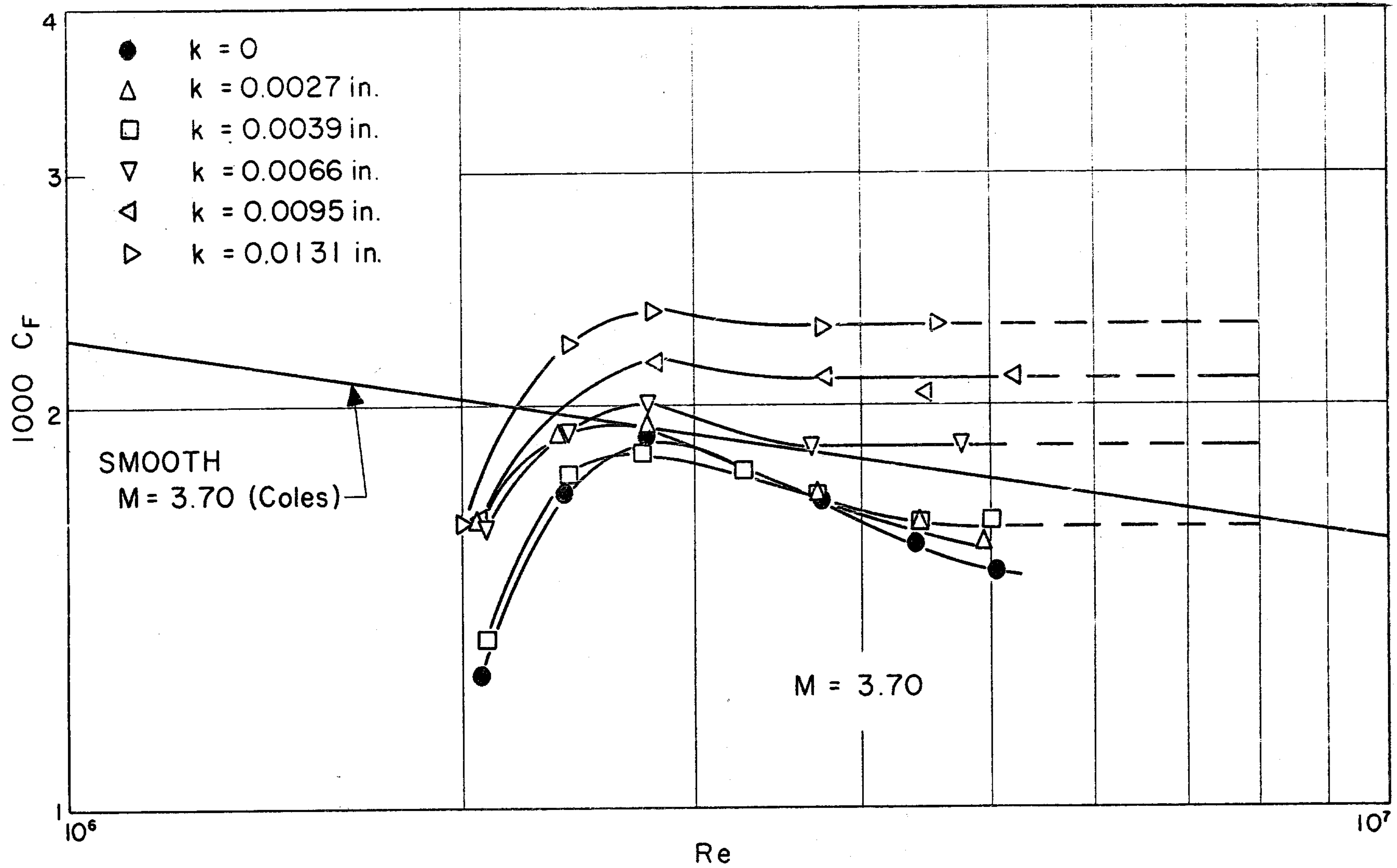

Figure 24. Average Skin Friction Drag Coefficient vs Reynolds Number - M = 3.70

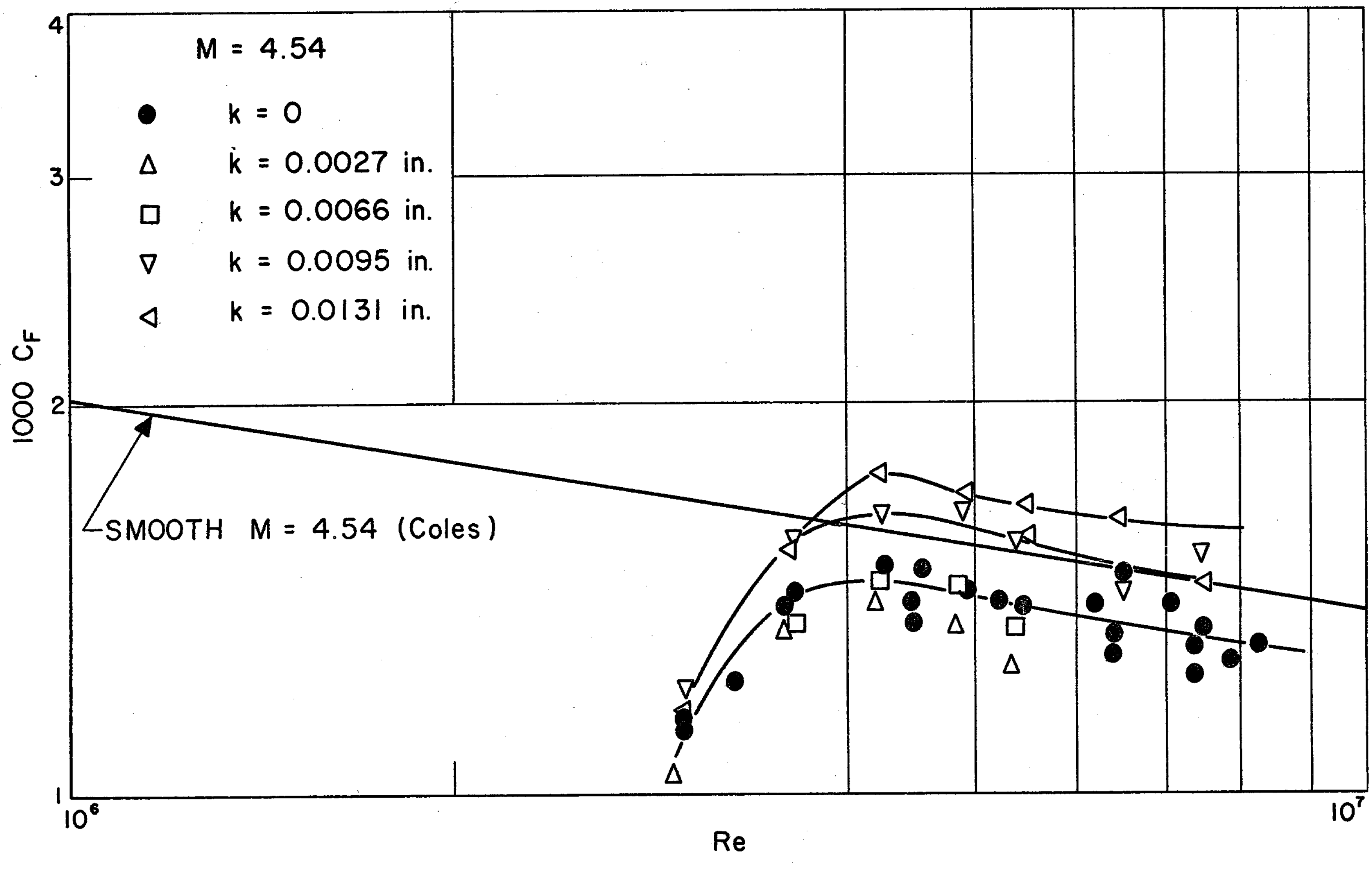

Figure 25. Average Skin Friction Drag Coefficient vs Reynolds Number - M = 4.54

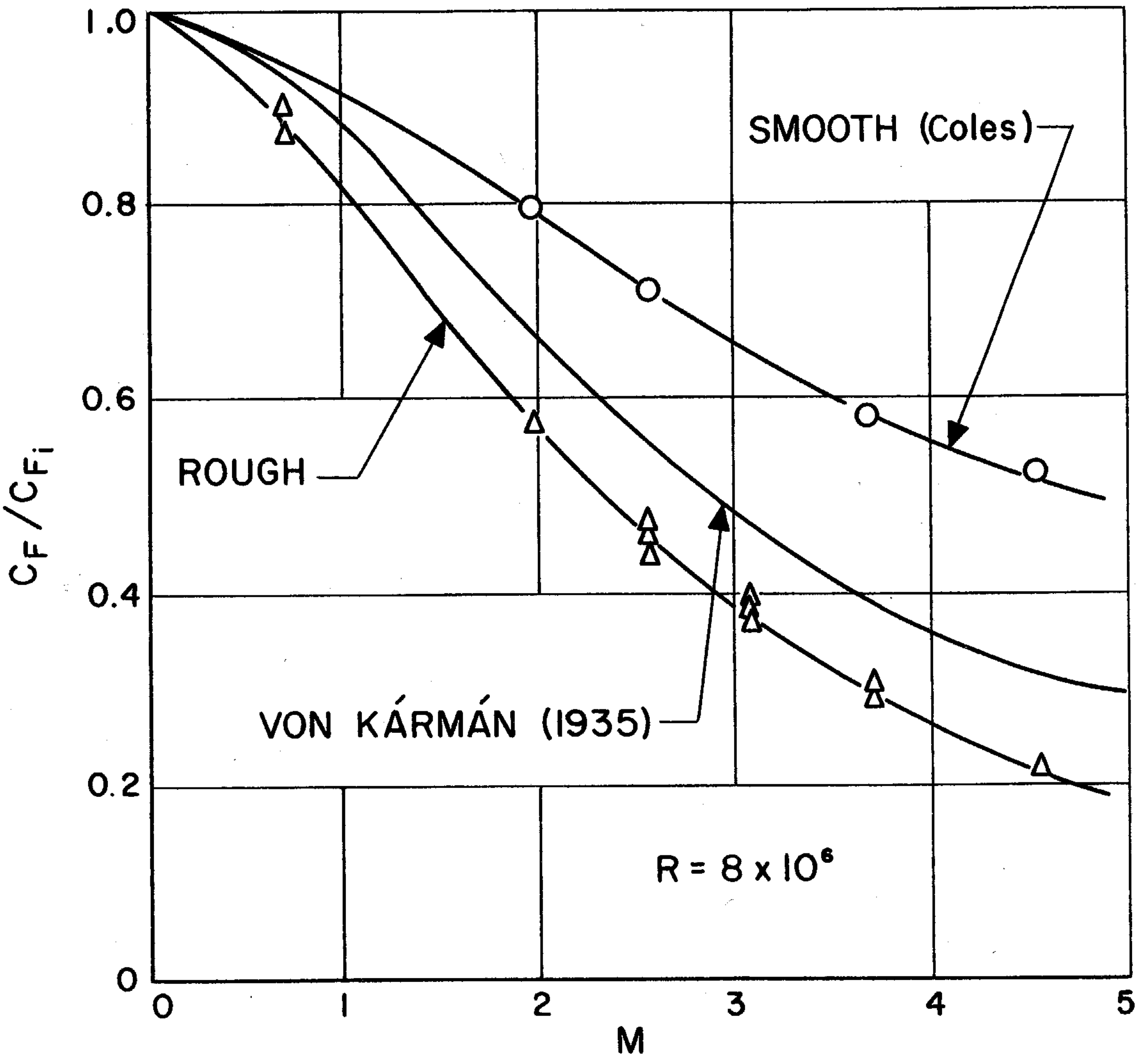

Figure 26. The Compressibility Effect on the Skin Friction Drag for Rough and Smooth Surfaces

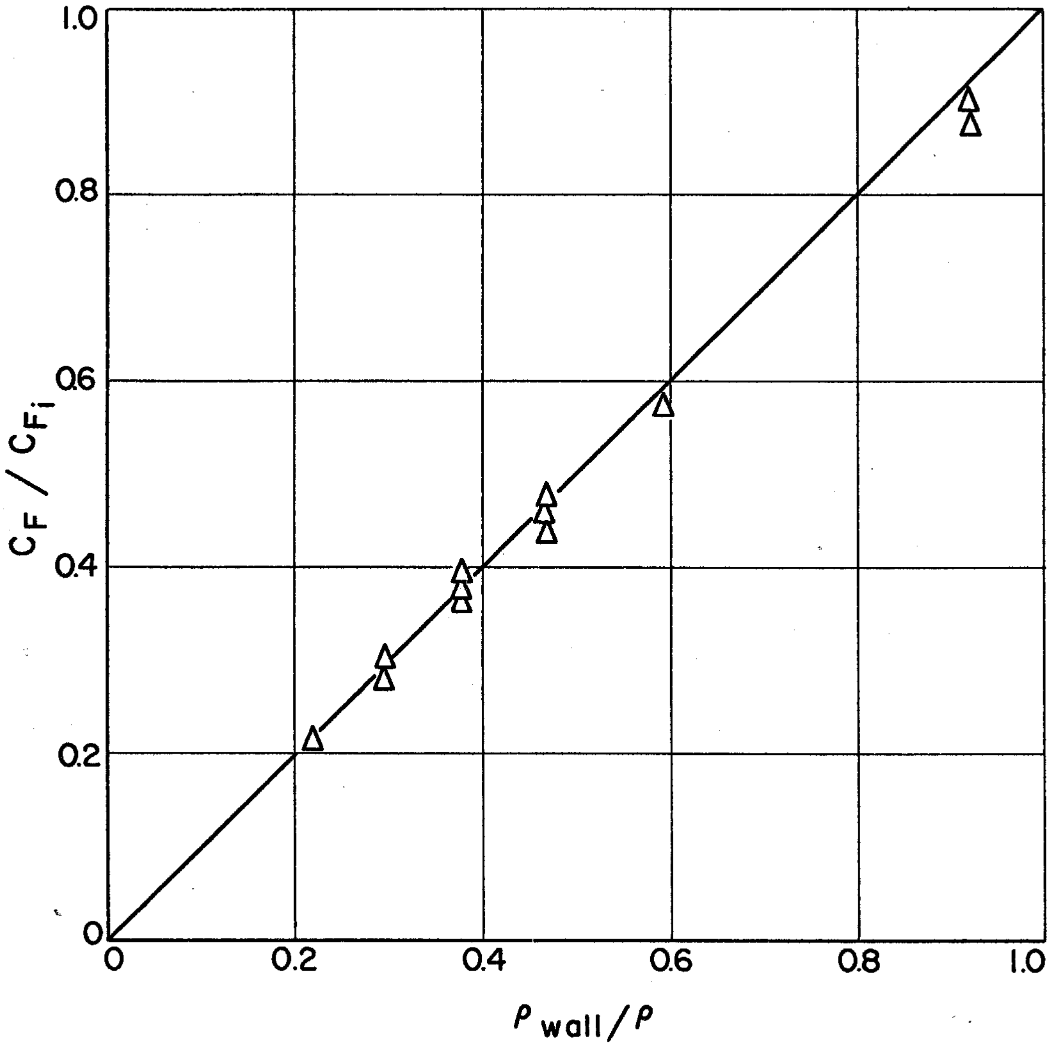

Figure 26a. Ratio of the Compressible to Incompressible Skin Friction Drag Coefficient for a Rough Surface vs the Ratio of Wall Density to Free-Stream Density

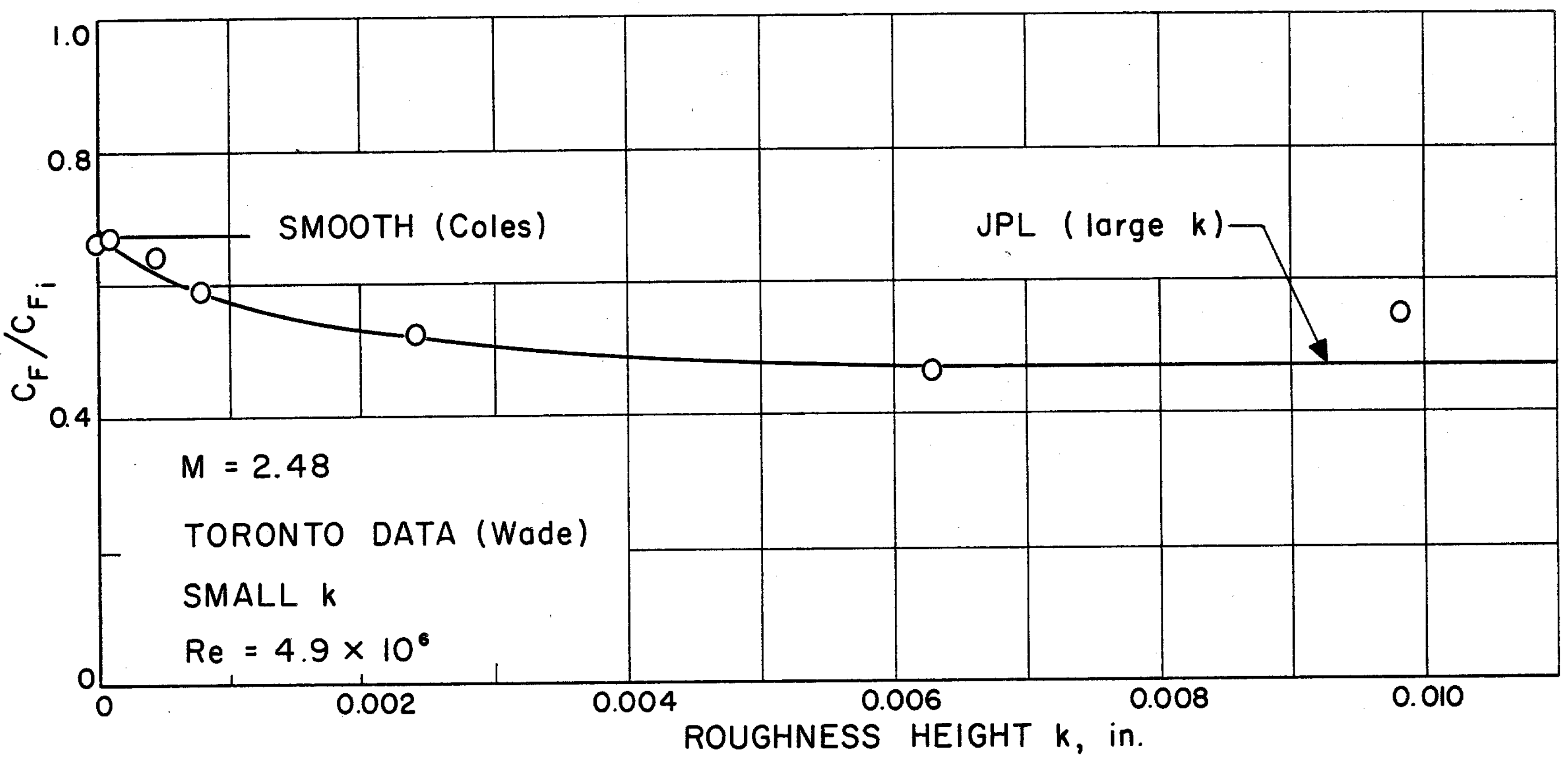

Figure 27. The Compressibility Effect vs Roughness Size - M = 2.48

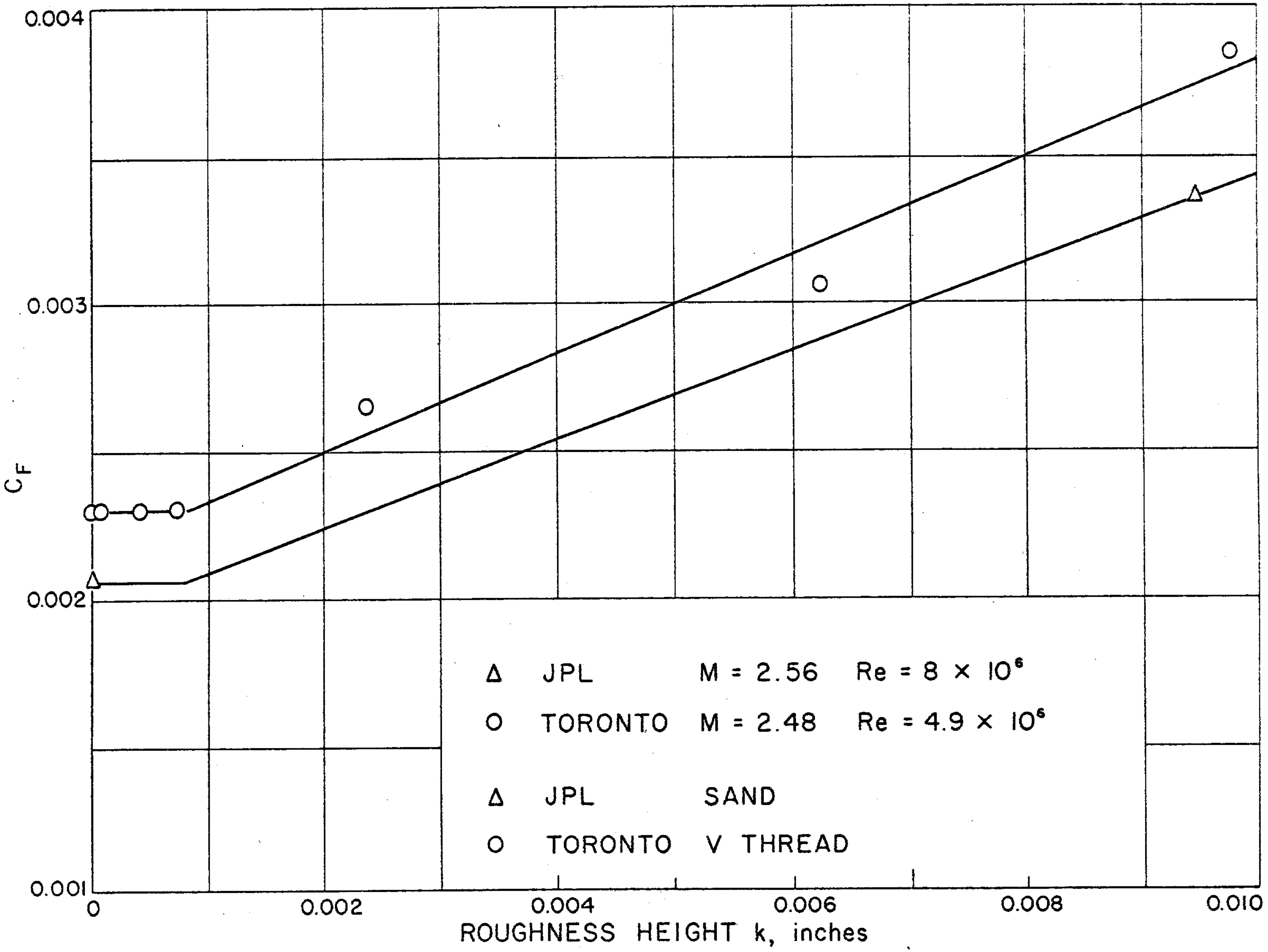

Figure 28. Average Skin Friction Drag Coefficient vs Roughness Height for Two Different Roughness Types

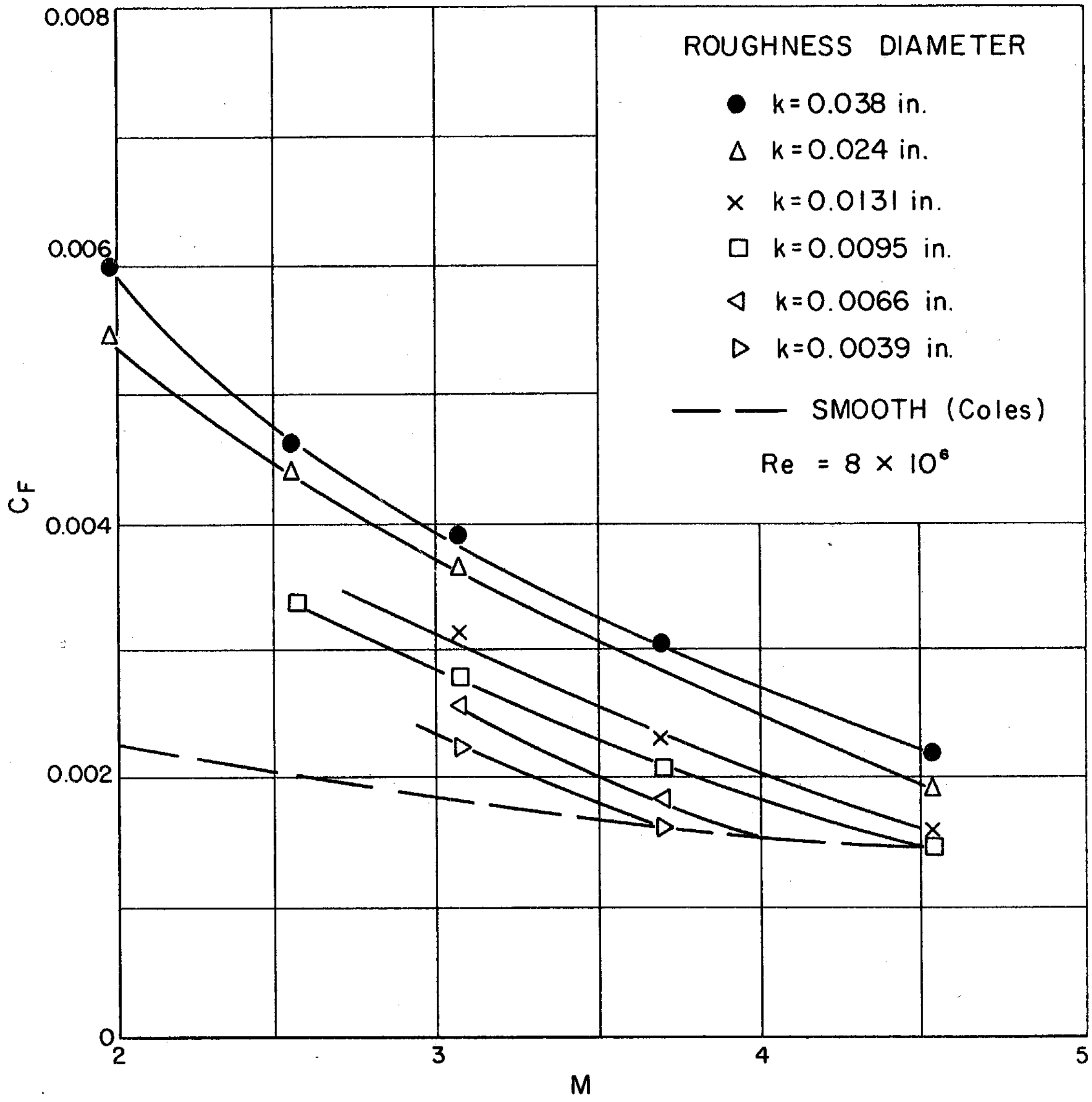

Figure 29. Average Skin Friction Drag Coefficient vs Mach Number for Various Roughness Heights

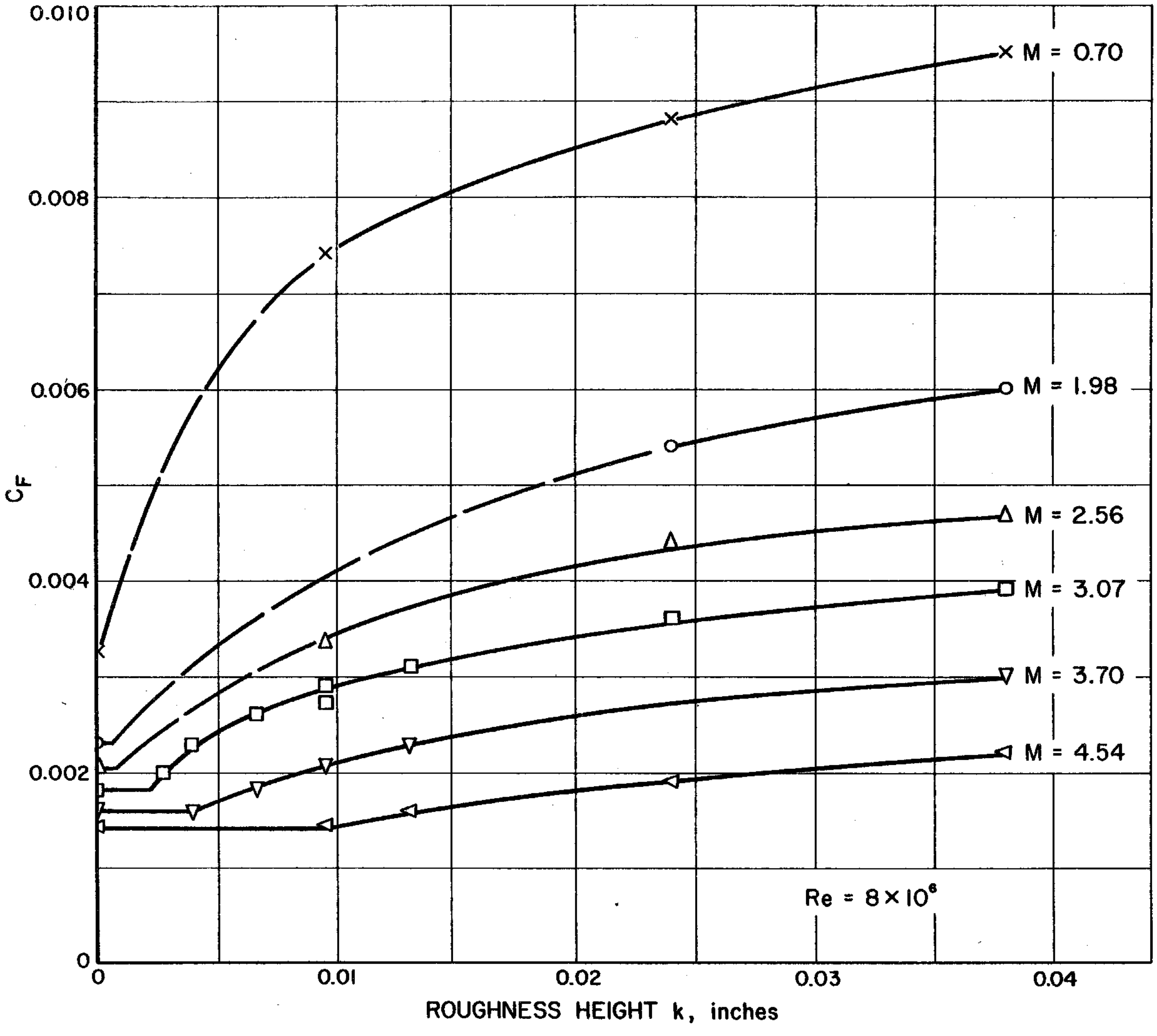

Figure 30. Average Skin Friction Drag Coefficient vs Roughness Height for Various Mach Numbers

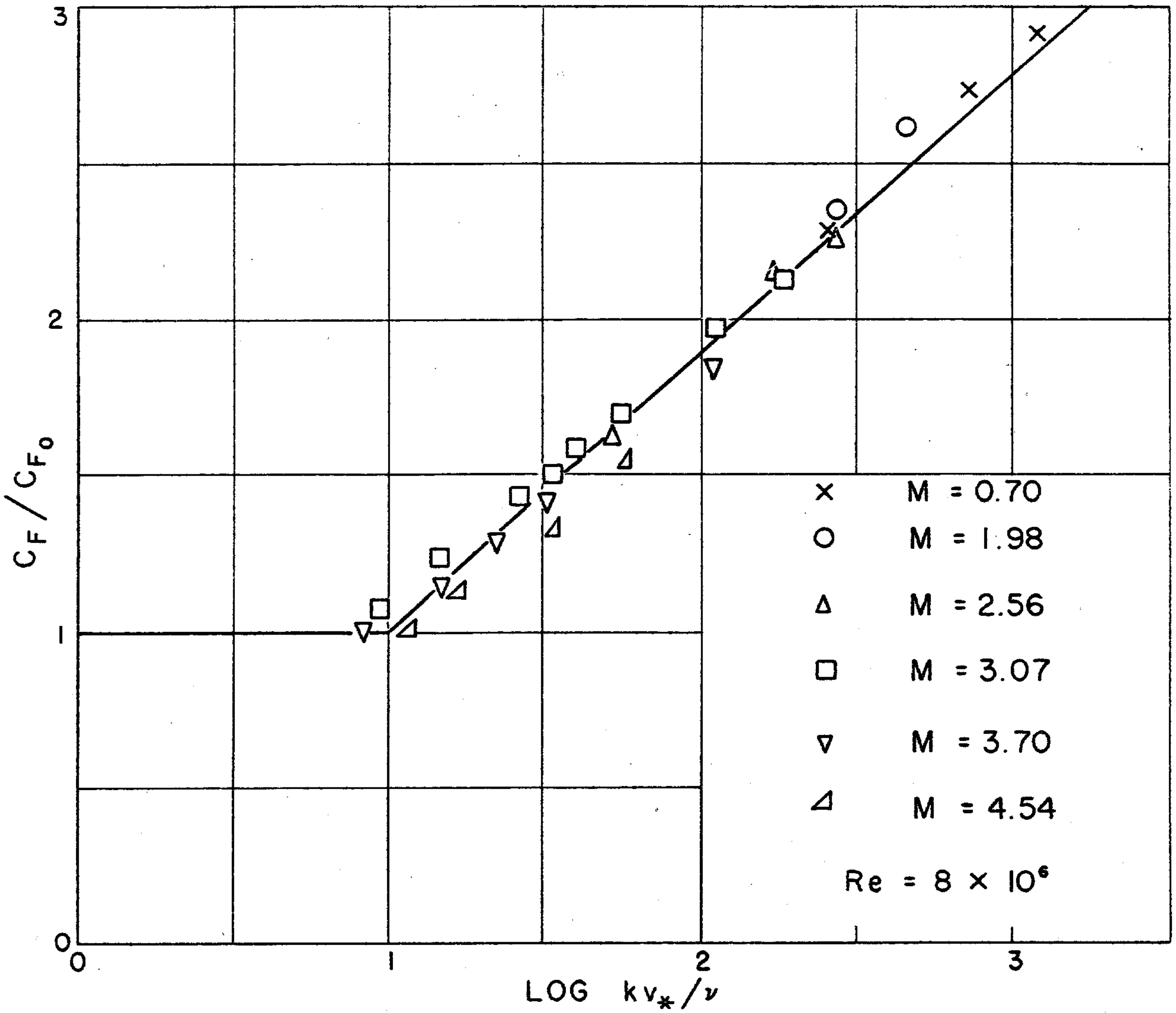

Figure 31. Ratio of the Skin Friction Drag Coefficient for a Rough Surface to that for a Smooth Surface vs Log $\frac{kv_*}{\nu}$

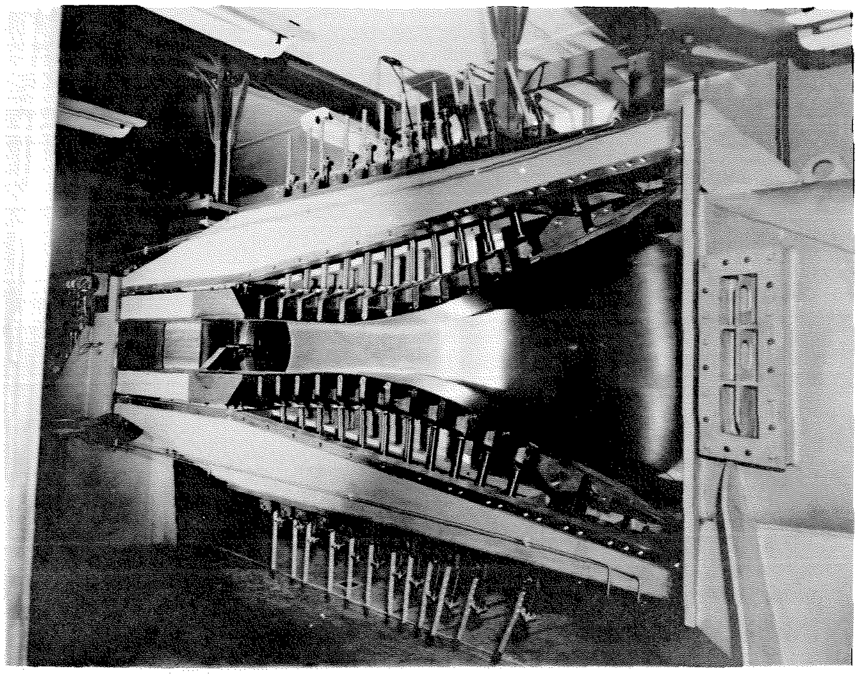

Figure 32. The JPL 12 × 12-Inch Supersonic Wind Tunnel

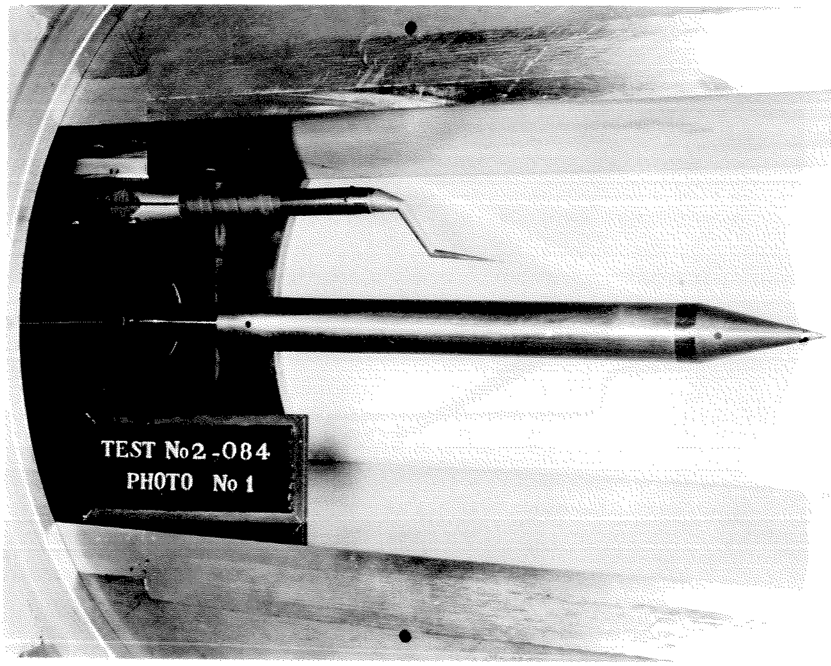

Figure 33. Model and Pitot Tube Installation for the Boundary-Layer Measurements

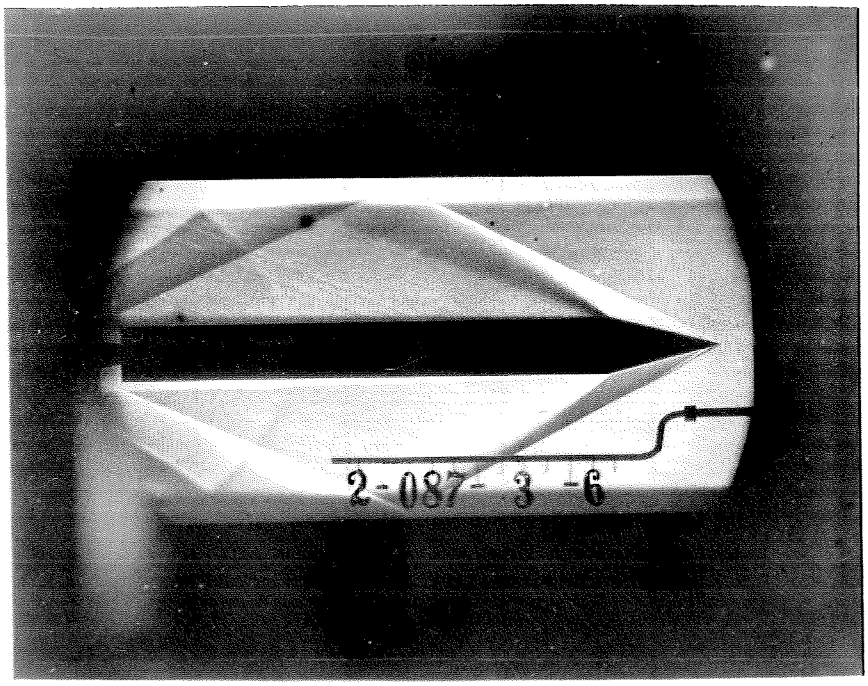

Figure 34. Schlieren Photograph of the Cone-Cylinder Model in the 12 × 12-Inch Tunnel

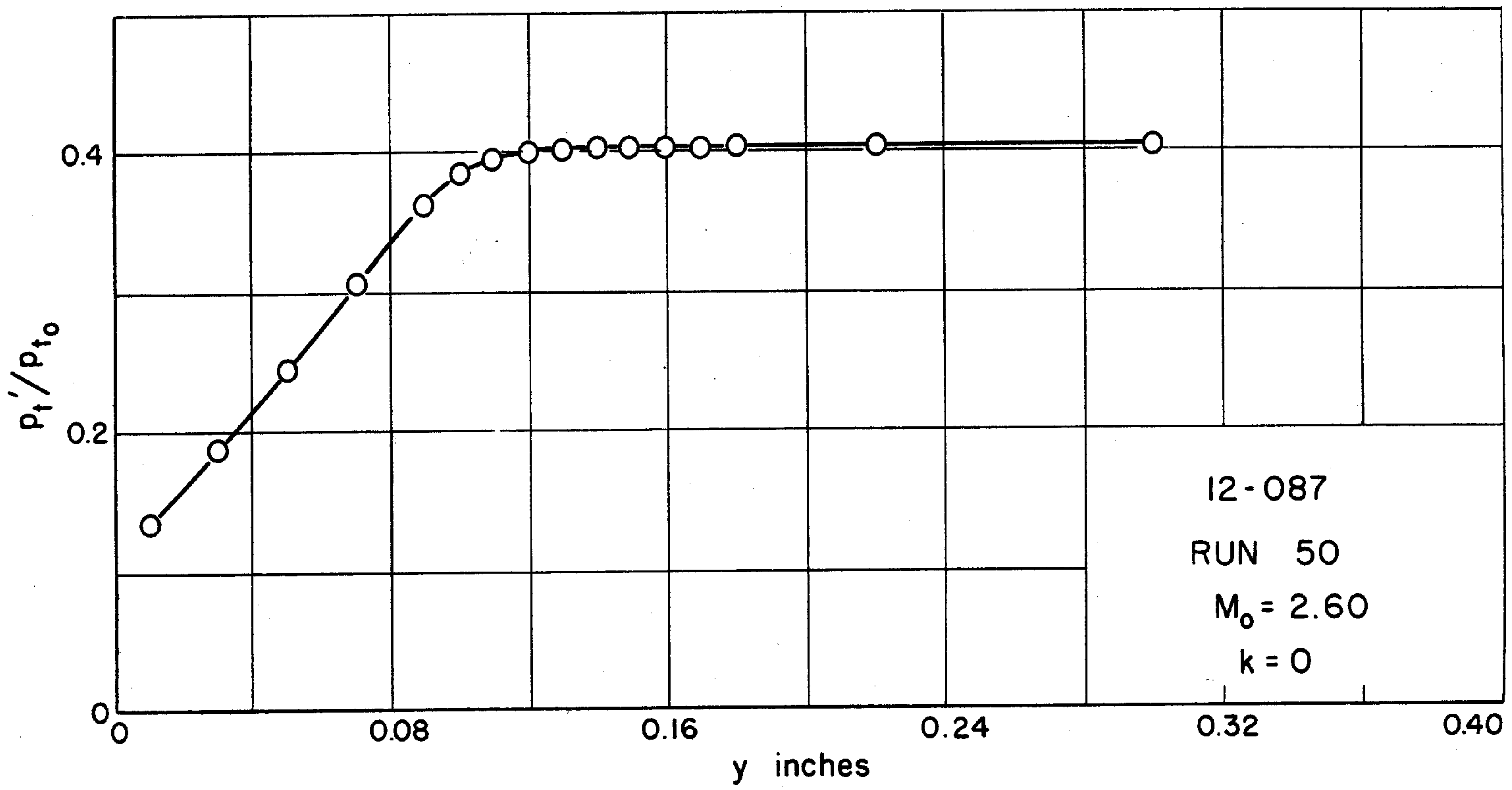

Figure 35. Pitot Pressure Profile in the Boundary Layer at $M_o = 2.60$ (k = 0)

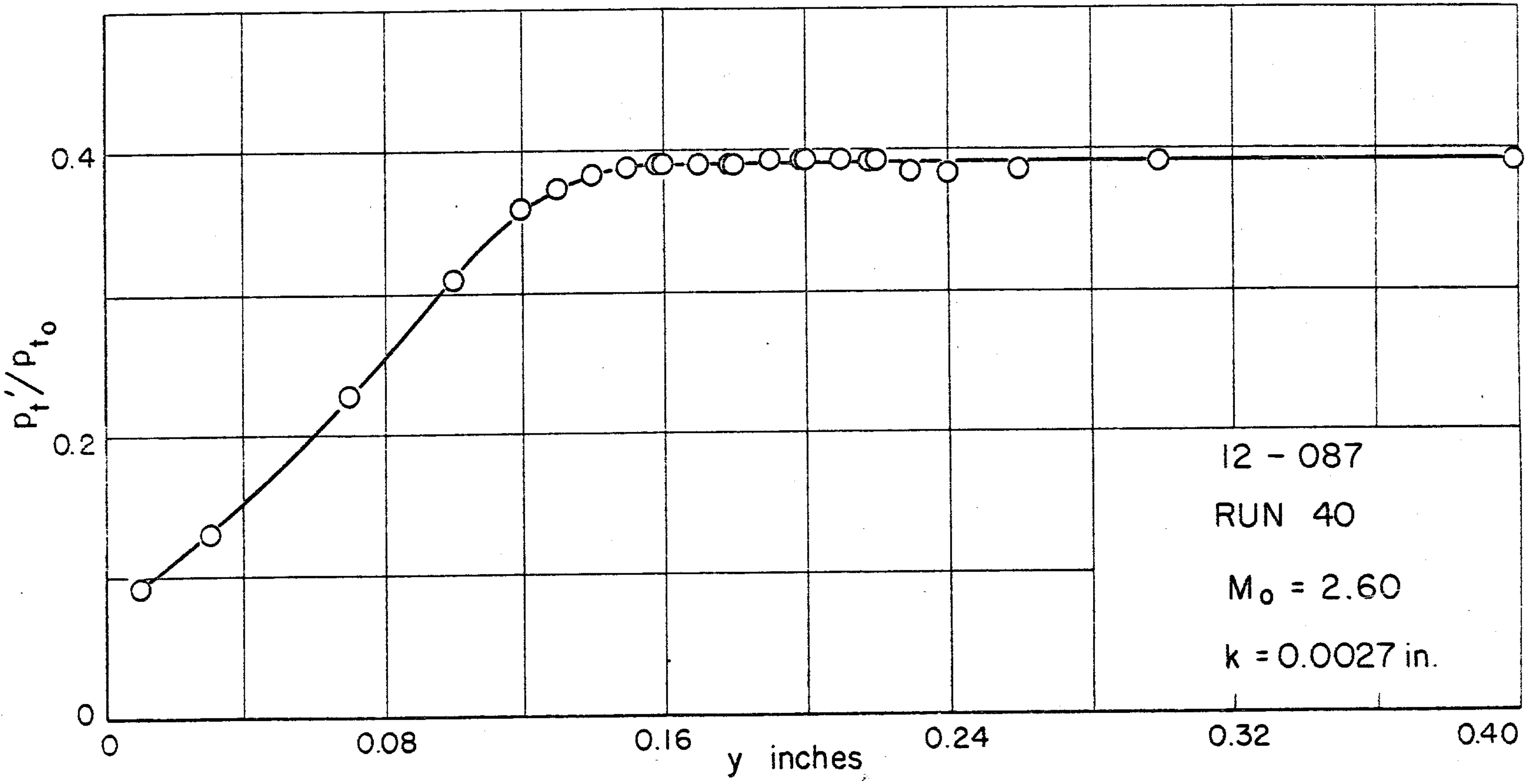

Figure 36. Pitot Pressure Profile in the Boundary Layer at $M_o = 2.60$ (k = .0027 in.)

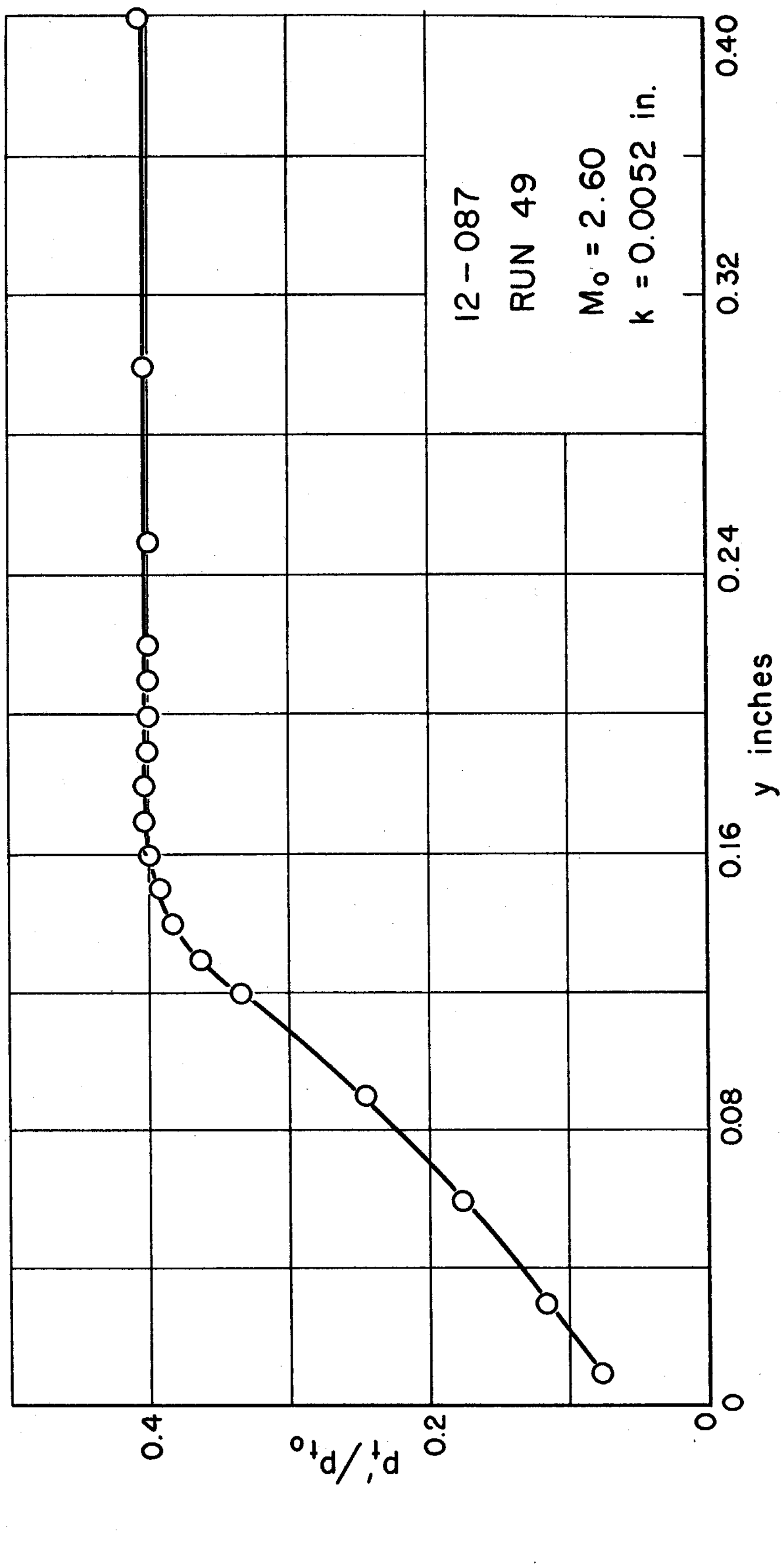

Figure 37. Pitot Pressure Profile in the Boundary Layer at $M_o = 2.60$ ($k = .0052$ in.)

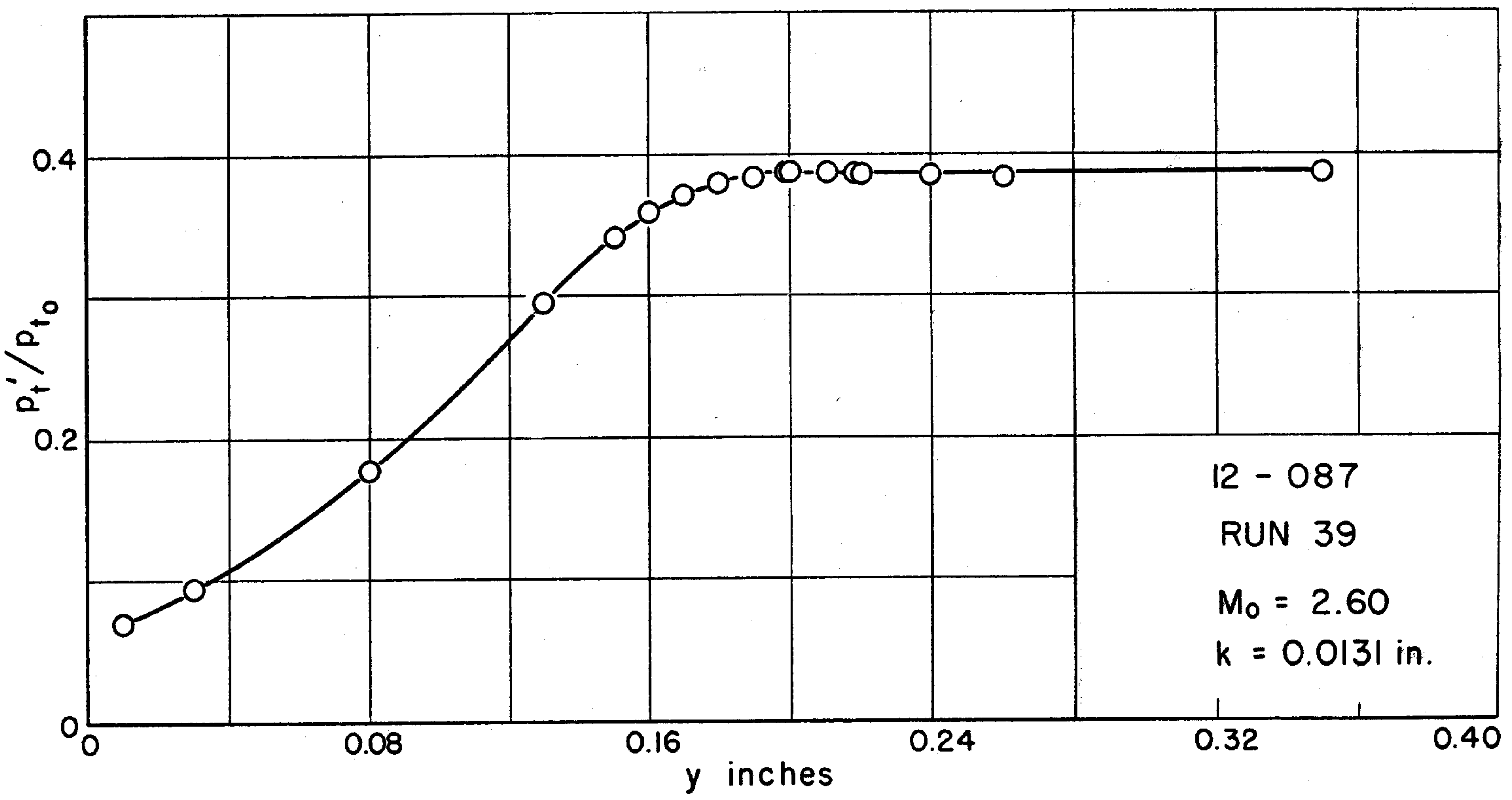

Figure 38. Pitot Pressure Profile in the Boundary Layer at M_o = 2.60 (k = .0131 in.)

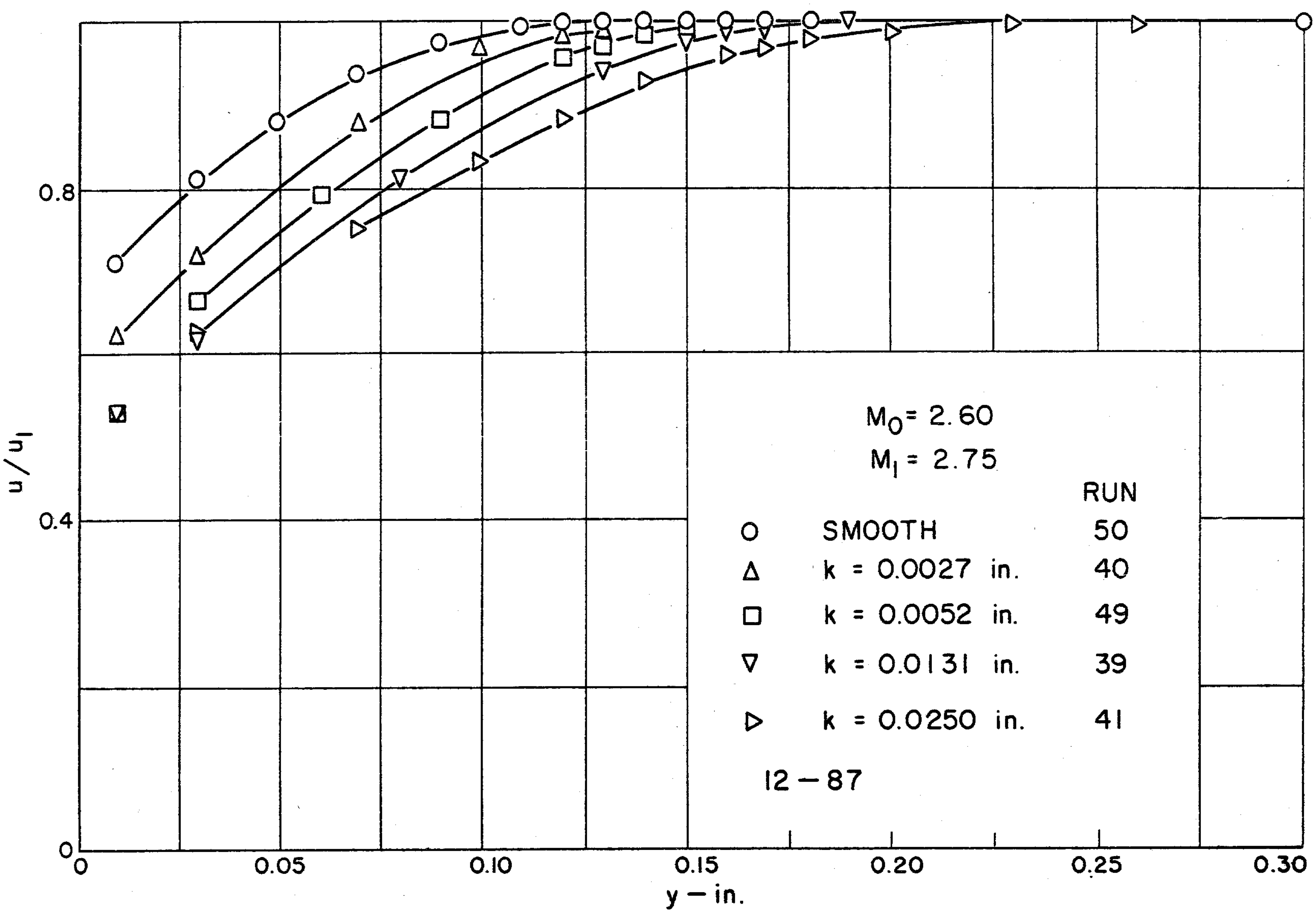

Figure 39. Velocity Profiles in the Boundary Layer at $M_o = 2.60$

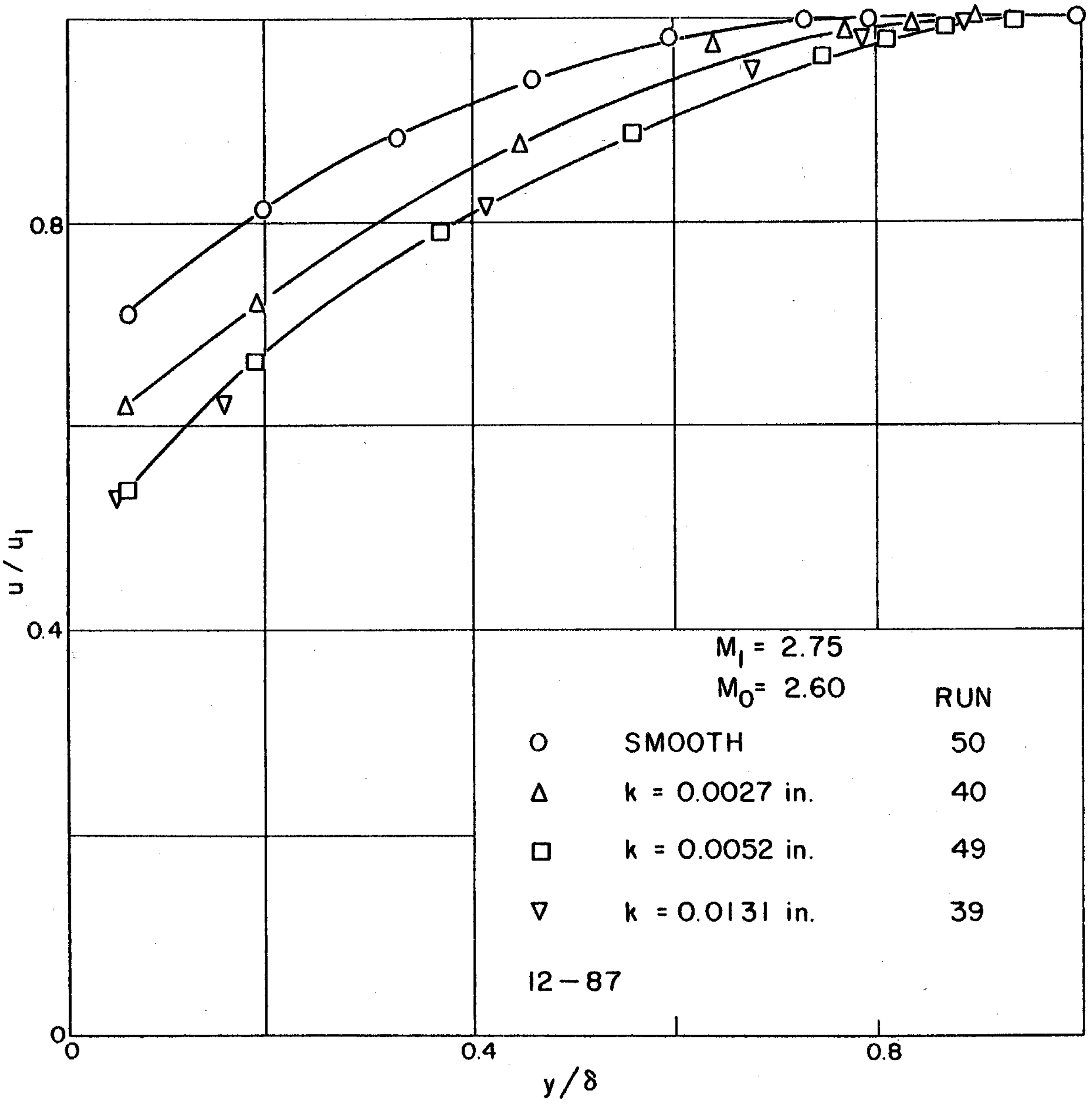

Figure 40. Velocity Profiles in the Boundary Layer at M_o = 2.60

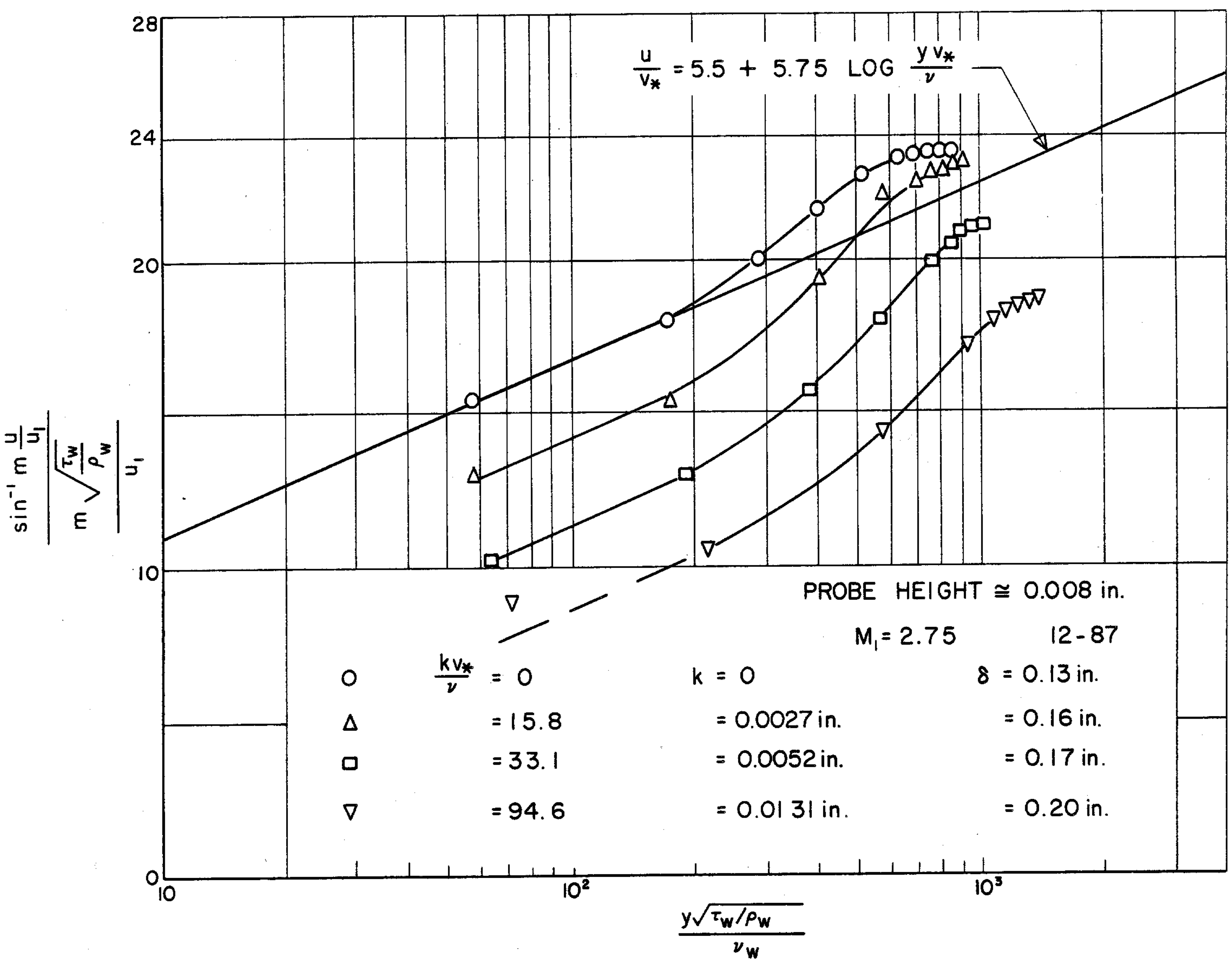

Figure 41. Nondimensional Velocity Profiles at M_o = 2.60

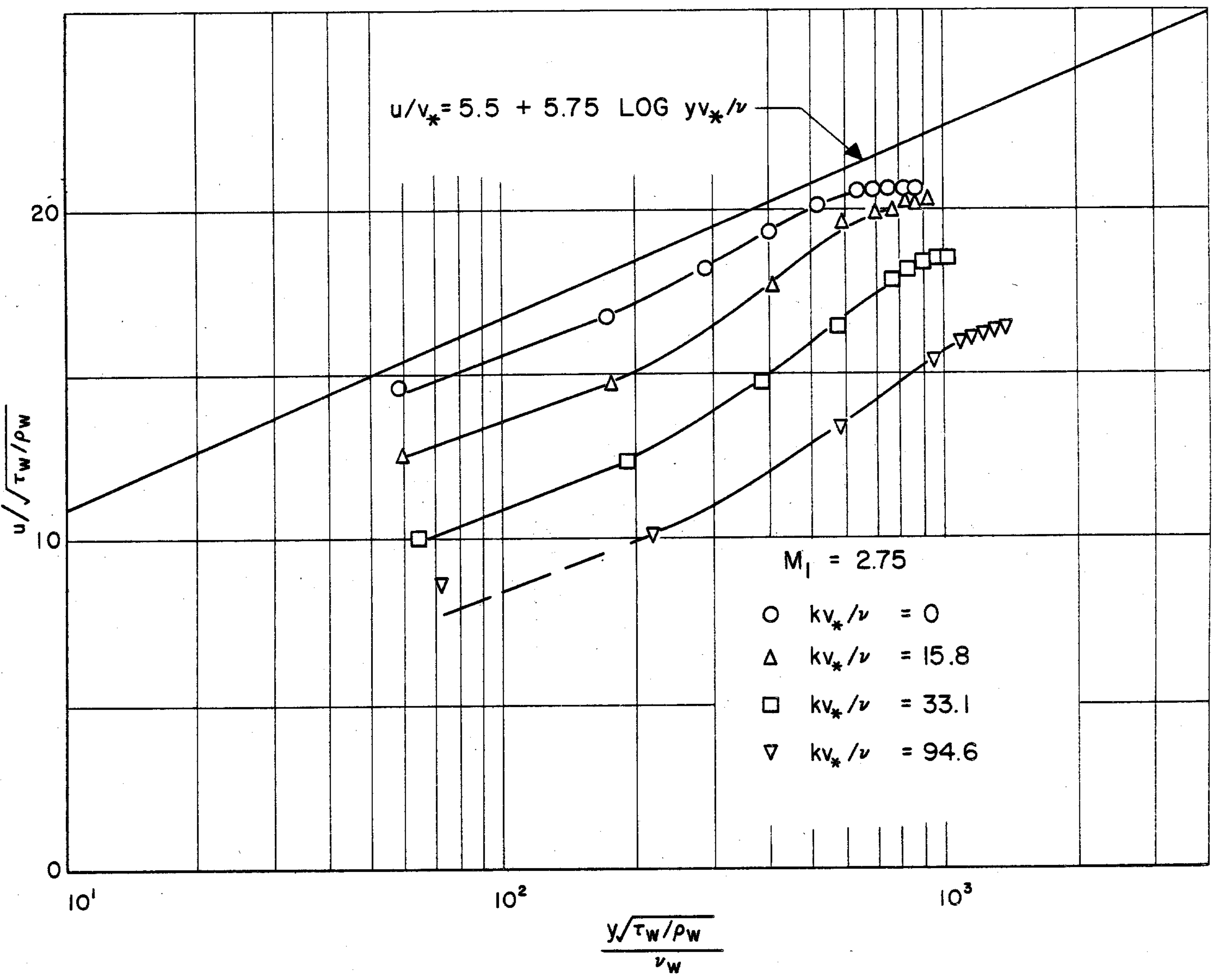

Figure 42. Nondimensional Velocity Profiles at $M_o = 2.60$

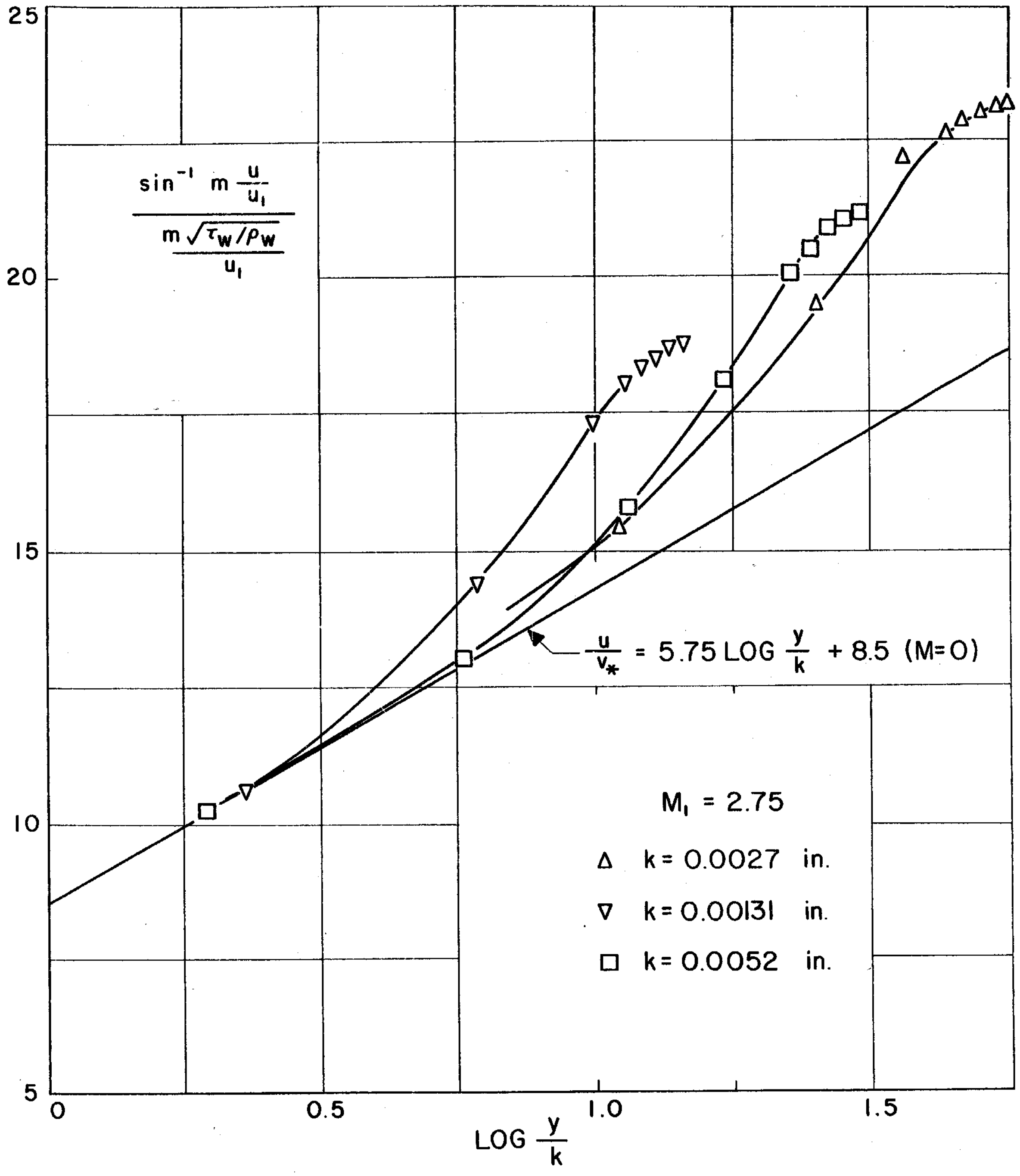

Figure 43. Nondimensional Velocity Profiles at M_o = 2.60

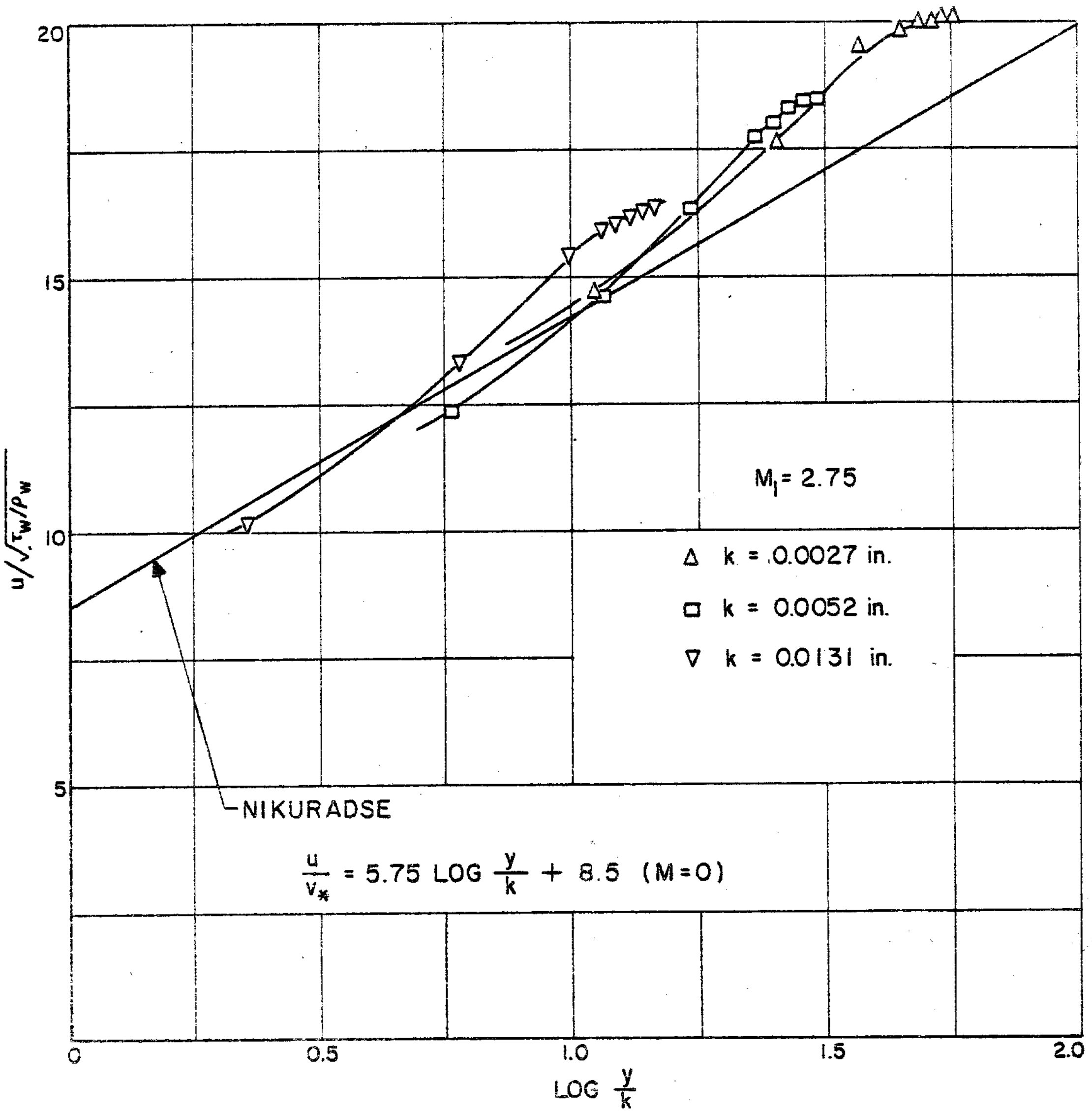

Figure 44. Nondimensional Velocity Profiles at M_o = 2.60

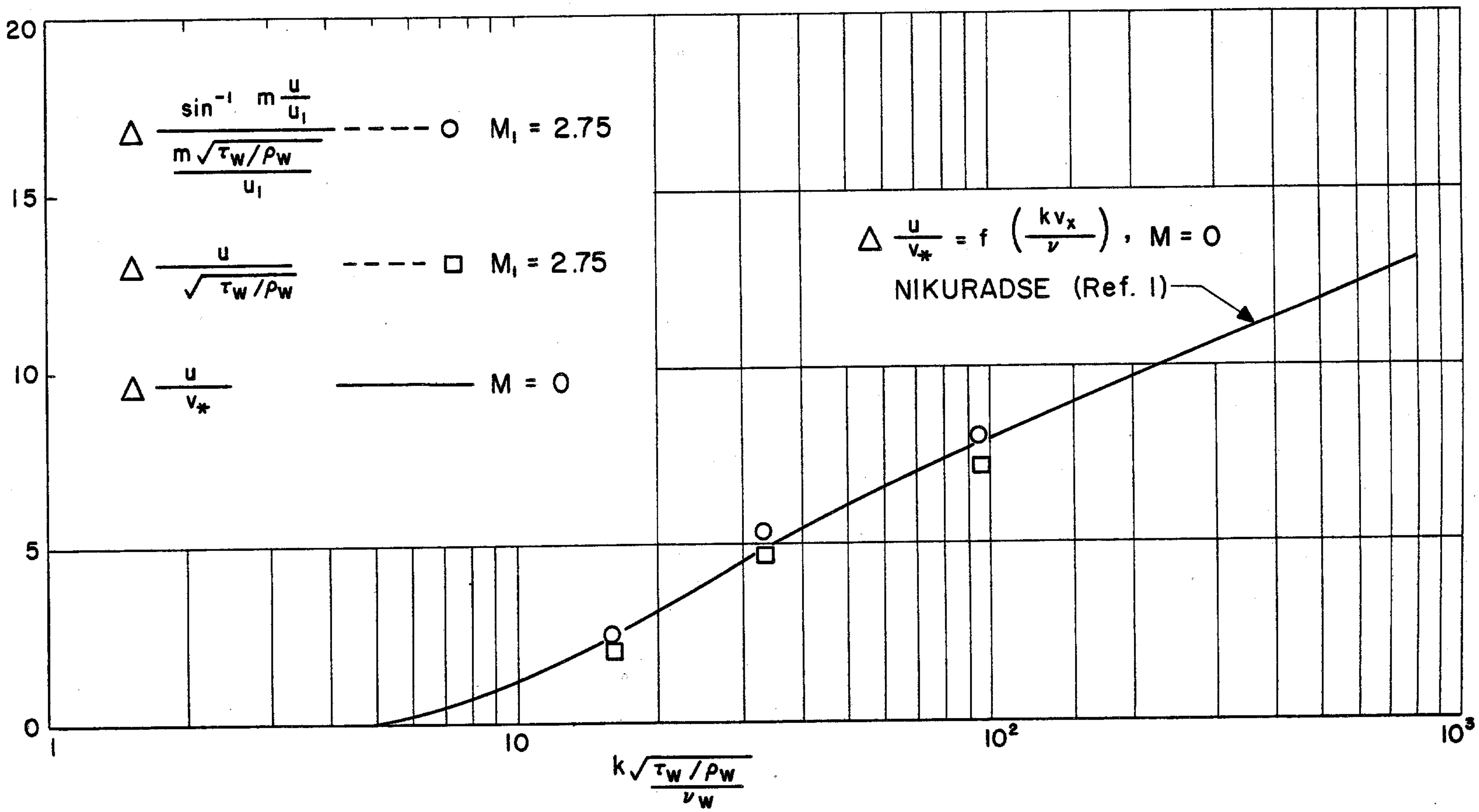

Figure 45. Effect of Roughness on the Velocity Profiles